ELUCIDATING THE MOLECULAR MECHANISMS OF *VIBRIO CHOLERAE* TOXIN COREGULATED PILUS ASSEMBLY, BUNDLING AND CTXϕ INTERACTIONS

by

Mindy S. Lim
B. Sc. (Hon.), Simon Fraser University, 2006

THESIS SUBMITTED IN PARTIAL FULFILLMENT OF
THE REQUIREMENTS FOR THE DEGREE OF

MASTER OF SCIENCE

In the Department of Molecular Biology and Biochemistry

SIMON FRASER UNIVERSITY

Spring 2009

APPROVAL

Name: **Mindy S. Lim**

Degree: **Master of Science**

Title of Thesis: **Elucidating the molecular mechanisms of *Vibrio cholerae* toxin coregulated pilus assembly, bundling and CTXϕ interactions**

Examining Committee:

Chair: **Dr. Nancy Forde**
Assistant Professor, Department of Physics

_____

Dr. Lisa Craig
Senior Supervisor
Assistant Professor, Department of Molecular Biology and Biochemistry

_____

Dr. Jamie K. Scott
Supervisor
Professor, Department of Molecular Biology and Biochemistry

_____

Dr. Fiona Brinkman
Supervisor
Associate Professor, Department of Molecular Biology and Biochemistry

_____

Dr. William S. Davidson
Internal Examiner
Professor, Department of Molecular Biology and Biochemistry

Date Defended/Approved: March 25th, 2009

Declaration of
Partial Copyright Licence

ABSTRACT

Vibrio cholerae use toxin-coregulated pili (TCP) to colonize the human intestine and cause severe diarrheal disease, cholera. TCP are surface filaments that self-aggregate to hold the bacteria in microcolonies that protect them from host defences and provide concentrated amounts of secreted cholera toxin. Also, TCP are receptors for a filamentous bacteriophage, CTXϕ, which carries the cholera toxin genes. To understand TCP assembly, TCP-mediated microcolony formation, and TCP:CTXϕ interactions at the molecular level, structure-based mutagenesis and functional assays were employed. I show charge complementarity between pilin subunits is important for initiating TCP assembly and hydrophobic interactions between subunits are required for pilus stability. I propose a model for pilus interactions whereby protruding regions of the TCP intercalate into depressions in adjacent TCP to form specific interactions that hold cells in microcolonies. Mutagenesis, immuno-gold electron microscopy analysis and functional assays suggest that CTXϕ attachment occurs over a large surface of TCP.

Keywords: *Vibrio cholerae*, Toxin co-regulated pilus, CTXϕ, microcolony formation, site directed mutagenesis, electron microscopy.

ACKNOWLEDGEMENTS

I am grateful for the guidance and support that Dr. Lisa Craig provided me with throughout the years. She broadened my knowledge and encouraged me to pursue my research through the ups and downs. Her insightful advice in the direction of my research brought me to where I am.

I thank my committee members, Dr. Jamie Scott and Dr. Fiona Brinkman, for their invaluable feedback on my research and setting time aside from their busy schedule.

I thank my internal examiner, Dr. William Davidson for all his support and invaluable advice he provided in completing my thesis.

Finally, my colleagues at Dr. Lisa Craig's lab for their help and encouragement and the laughs we shared.

TABLE OF CONTENTS

LIST OF FIGURES

LIST OF TABLES

GLOSSARY

AA	Autoagglutination
ADP	Adenosine diphosphate
Amp	Ampicillin
cAMP	Cyclic adenosine monophosphate
cfu	Colony forming unit
CT	Cholera toxin
CTXϕ	Cholera toxin phage
DNA	Deoxyribonucleic acid
Gm	Gentamicin
IMP	Integral inner membrane protein
IPTG	Isopropyl-beta-D-thiogalactopyranoside
Kan	Kanamycin
PAGE	Polyacrylamide gel electrophoresis
PBS	Phosphate buffered saline
PCR	Polymerase chain reaction
PKA	Protein Kinase A
PTA	Phosphotungstic acid
RF	Replicative form
SDS	Sodium dodecyl sulphate

Sm	Streptomycin
ssDNA	Single stranded DNA
TBS	Tris (hydroxymethyl) methylamine buffered saline
TEM	Transmission electron microscopy
TCP	Toxin coregulated pilus/pili
X-gal	5-bromo-4-choloro-3-indolyl-β-D-galactoside

CHAPTER 1: INTRODUCTION

1.1 *Vibrio cholerae*

The Gram-negative bacterium *Vibrio cholerae* causes the acute life-threatening diarrheal disease cholera. Cholera has afflicted human populations in many parts of the world for more than a millennium (Barua *et al*., 1992). While cholera has been virtually eradicated in industrialized countries, cholera still afflicts people in developing countries where accessibility to clean water and sanitation is limited. Recent data show that cholera is re-emerging with an increasing proportion of vulnerable populations living in unsanitary conditions (World Health Organization, 2007). In 2006, over 240,000 cases from 52 countries were reported to World Health Organization (WHO), which is 79% increase from the previous year. However, this number is believed to be grossly underestimated as thousands of cases, mostly from central and south Asia, are never reported officially (WHO, 2007). Globally, an estimated 120,000 deaths from cholera occur each year (WHO, 2001).

There are over 200 different *V. cholerae* serogroups but only two are associated with severe disease and cholera pandemics: serogroups O1 and O139 (Chatterjee *et al*., 2003; Wachsmuth *et al*., 1994). *V. cholerae*, including pandemic strains, are part of the normal aquatic flora in estuarine and brackish waters (Colwell *et al*., 1977; Colwell *et al*., 1994; Garay *et al*., 1985; Islam *et al*., 1994). Within the marine environment they attach to the surfaces of plants,

filamentous green algae, copepods (zooplankton), crustaceans, and insects (Colwell *et al*., 1994; Garay *et al*., 1985; Islam *et al*., 1994; Huq *et al*., 1990).

Serogroup O1 is divided into two biotypes, classical and El Tor, which together are responsible for all seven of the major cholera disease pandemics during the last 200 years (Barua *et al*., 1992). The classical biotype was the causative agent of cholera until the early 1960s when it was replaced by the El Tor biotype, which is also responsible for the ongoing cholera epidemic that started in Zimbabwe last year (WHO, 2008). More than 60,000 people have been infected in this most recent epidemic, which is not yet under control and has already killed over 3,000 people (WHO, 2009). The cause of biotype switch in cholera outbreaks is not known. The two biotypes, classical and El Tor, have traditionally been differentiated in the laboratory with assays of hemolysis, hemagglutination, phage sensitivity, and polymyxin sensitivity and with the Voges-Proskauer reaction. Genetic typing of strains has also become possible in recent years. However, despite their phenotypic and genotypic differences, the symptoms of infection with strains of the two O1 biotypes are clinically indistinguishable (Kaper *et al*., 1995).

1.2 Pathogenesis

V. cholerae pathogenesis is a complex process that can be divided into three stages (Figure 1.1). Infection involves a number of virulence factors which aid the pathogen in its passage to reach the epithelium of the small intestine, colonize the epithelium, and produce a potent enterotoxin that disrupts ion transport by intestinal epithelial cells (Kaper *et al*., 1995). The two most important

virulence factors in *V. cholerae* include the cholera toxin (CT) which is primarily responsible for the acute diarrhea, and a colonization factor known as the toxin coregulated pilus (TCP), named as its expression is under the same genetic control as that of CT (Taylor *et al*., 1987).

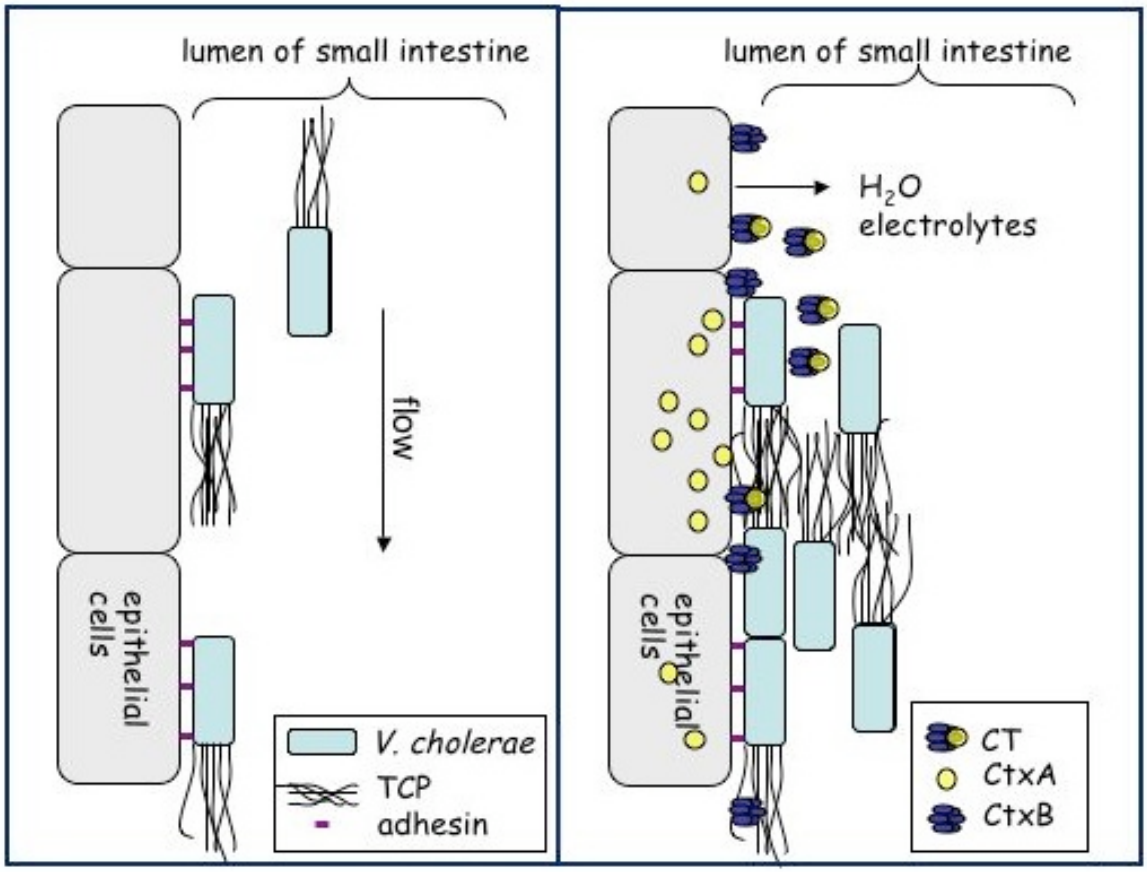

Figure 1.1 Overview of *V. cholerae* infection process. *V. cholerae* attaches to intestinal wall of epithelial cells via GbpA and other adhesins. TCP mediates microcolony formation and *V. cholerae* secrets CT. This results in loss of fluids and electrolytes from the epithelial cells and surrounding tissues.

CT acts as a classical AB_5 toxin that ribosylates ADP of a small G protein, which leads to the constitutive activation of adenylate cyclase. This results in increased levels of cyclic AMP (cAMP) within the host cell. cAMP activates

protein kinase A (PKA) which in turn activates chloride channels. This leads to rapid efflux of chloride and sodium ions and water from host intestinal cells, causing diarrhea and vomiting (Figure 1.2). This massive outpouring of fluid and electrolytes leads to severe dehydration, electrolyte abnormalities and metabolic acidosis (Kaper *et al*., 1995).

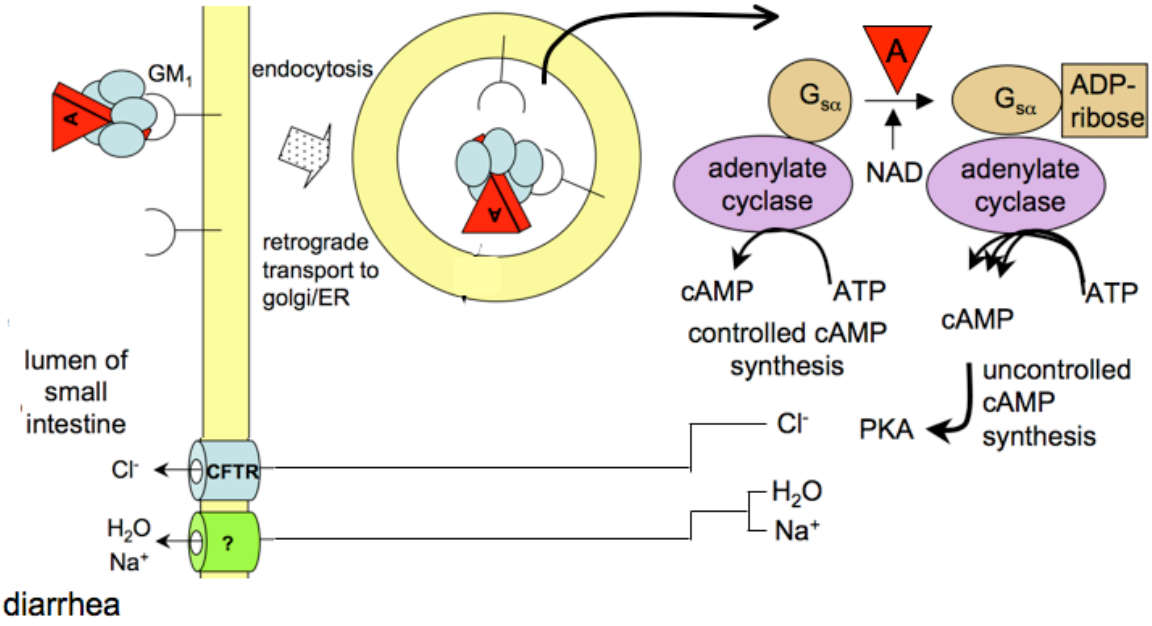

Figure 1.2 **Mode of action of cholera toxin.** Adenylate cyclase located in the basolateral membrane of intestinal epithelial cells is regulated by G proteins. CT binds to the GM1 ganglioside via its B subunit and is taken up by the cell via endocytosis. The A subunit of CT catalyzes the transfer of ADP-ribose from NAD to the α-subunit of the G protein. This leads to uncontrolled cAMP synthesis, and activates protein kinase A (PKA), which activates water and electrolyte channels. This leads to massive efflux of chloride and sodium ions and water from intestinal cells resulting in severe dehydrating diarrhea.

The TCP play an equally crucial role in *V. cholerae* pathogenesis, having three key functions in virulence: i) TCP adhere to each other to hold the *Vibrio* cells in microcolonies (Figure 1.3), protecting them from the harsh environment of

the small intestine and concentrating the secreted cholera toxin at the site of colonization (Herrington *et al*.,1988); (ii) TCP is the high affinity receptor for the cholera toxin phage, CTXϕ, which confers toxicity on *V. cholerae* as it provides the genes that encode the cholera toxin subunits, A and B (Waldor *et al*.,1996); and (iii) the TCP biogenesis apparatus acts as a secretion system, exporting a newly-recognized virulence factor, TcpF, which is also necessary for *V. cholerae* colonization (Kirn *et al*., 2003). In the absence of TCP, *V. cholerae* fail to colonize the human gut, thus highlighting TCP's central role in pathogen-host interactions (Herrington *et al*.,1988; Tacket *et al*.,1998).

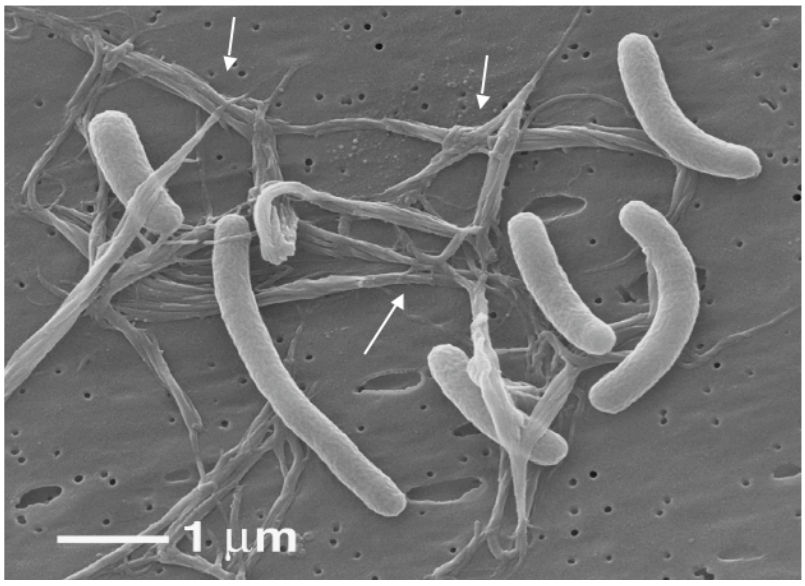

Figure 1.3 Microcolony formation is mediated by toxin coregulated pili (TCP). *Vibrio* cells are held together by the TCP (indicated by an arrow). Photo courtesy of Ronald K. Taylor, Dartmouth Medical School, USA.

1.3 TCP

V. cholerae TCP belong to the Type IV pilus family. Type IV pili are polymers of helically arranged pilin subunits present on many Gram-negative bacteria, including the human pathogens *Neisseria gonorrhoeae, N. meningitidis, Pseudomonas aeruginosa,* and enterotoxigenic and enteropathogenic *Escherichia coli*. Type IV pili are key virulence factors, mediating various functions including twitching motility, adherence, antigenic variation and colonization (Craig *et al*., 2004). Like *V. cholerae, N. gonorrhoeae, N. meningitidis* and enteropathogenic *E. coli* use Type IV pili to mediate microcolony formation in addition to other functions (Bieber *et al*.,1998; Higashi *et al*., 2007; Marceau *et al*., 1995).

The subunits of Type IV pili share amino acid sequence homology and have a conserved set of assembly components within the pilus assembly apparatus (Craig *et al*., 2004). All Type IV pilins have an N-methylated N-terminal residue, conserved hydrophobic N-terminal 25 residues, and a conserved pair of C-terminal cysteines.

Several atomic structures of Type IV pilin subunits have been determined (Figure 1.4). Comparison of these structures revealed a ladle shaped structure with an extended N-terminal α-helix, α1, and a globular head domain. The globular head domain is formed by the C-terminal half of the α1, α1C, and anti-parallel β-sheets. The greatest length, sequence and structural variability among Type IV pilins are found in $\alpha\beta$-loop and D-regions. The $\alpha\beta$-loop lies between the N-terminal α-helix and the C-terminal β-sheet, and the D-region lies within the

disulfide bridge formed by the two conserved cysteines (Figure 1.4). The crystal structures of the N-terminally truncated pilin subunit TcpA, was solved from both classical and El Tor biotypes (Figure 1.4; Craig *et al*., 2003; Lim *et al*., manuscript in preparation). These crystal structures lack the first 28 hydrophobic N-terminal residues of the subunit as this segment makes pilin subunit insoluble, making crystallization extremely difficult. TcpA from the two biotypes share 81% amino acid sequence identity and have virtually identical protein folds and side chain conformations. Residues 1-28 are predicted to form an extended, protruding α-helix, α1N, based on sequence homology with the full length *P. aeruginosa* PAK pilin structure (Craig *et al*., 2003).

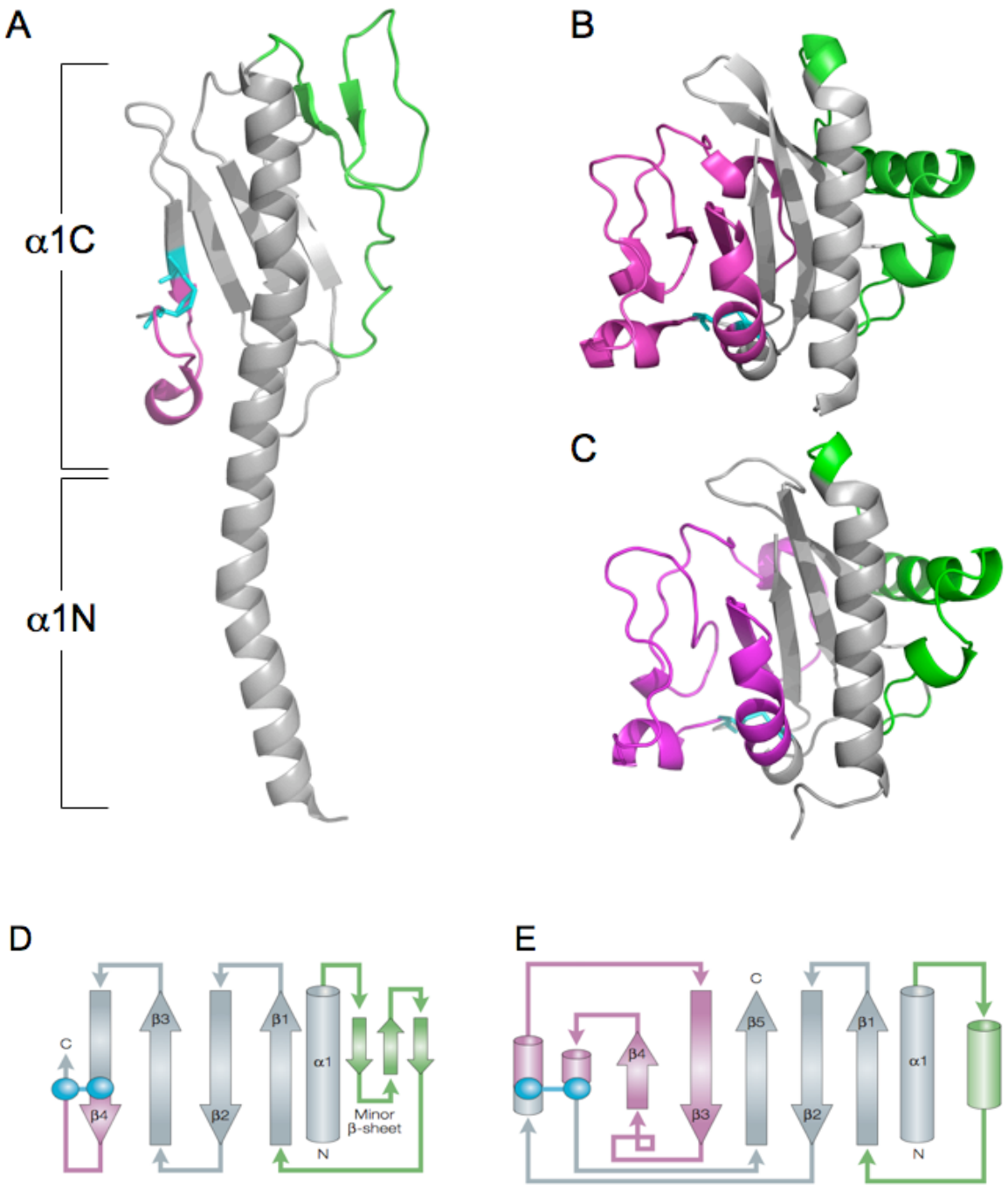

Figure 1.4 **Structural comparison of the Type IV pilins.** Structure of (A) full-length PAK pilin (PDB accession number 10QW) (B) N-terminally truncated *V. cholerae* TcpA from classical biotype (1.3 Å; PDB accession number 10QV) and (C) El Tor biotype (1.5 Å). (D) Secondary structure diagrams of PAK pilin and (E) TcpA. In each of structures, the αβ-loop is coloured green, the D-region is coloured magenta and the disulphides are coloured cyan.

A computational filament model of TCP from the classical *V. cholerae* biotype was generated based on the subunit crystal structure, crystallographic packing, filament dimensions and helical symmetry determined by analysis of cryo-electron microscopy images (Craig *et al*., 2003). The atomic coordinates of the N-terminal 28 residue of the full-length PAK pilin structure from *P. aeruginosa* was used to position α1N of TcpA. Recently this computational model was refined based on solvent accessibility measured by deuterium exchange mass spectrometry (Li et *al*., 2008). An El Tor TCP filament model was generated by fitting the El Tor TcpA structure into the classical TCP model (Lim *et al*., manuscript in preparation). This model revealed that the TCP filament has an undulating surface with substantial gaps between the TcpA subunits that expose a segment of the N-terminal α-helix, and bulges at the C-terminal region of TcpA (Figure. 1.5). Based on this computational filament model and on a comparison of the classical and El Tor TcpA subunits, discrete regions of the TcpA subunit predicted to be involved in pilus assembly, microcolony formation and pilus:CTXϕ interactions were chosen for mutational analysis.

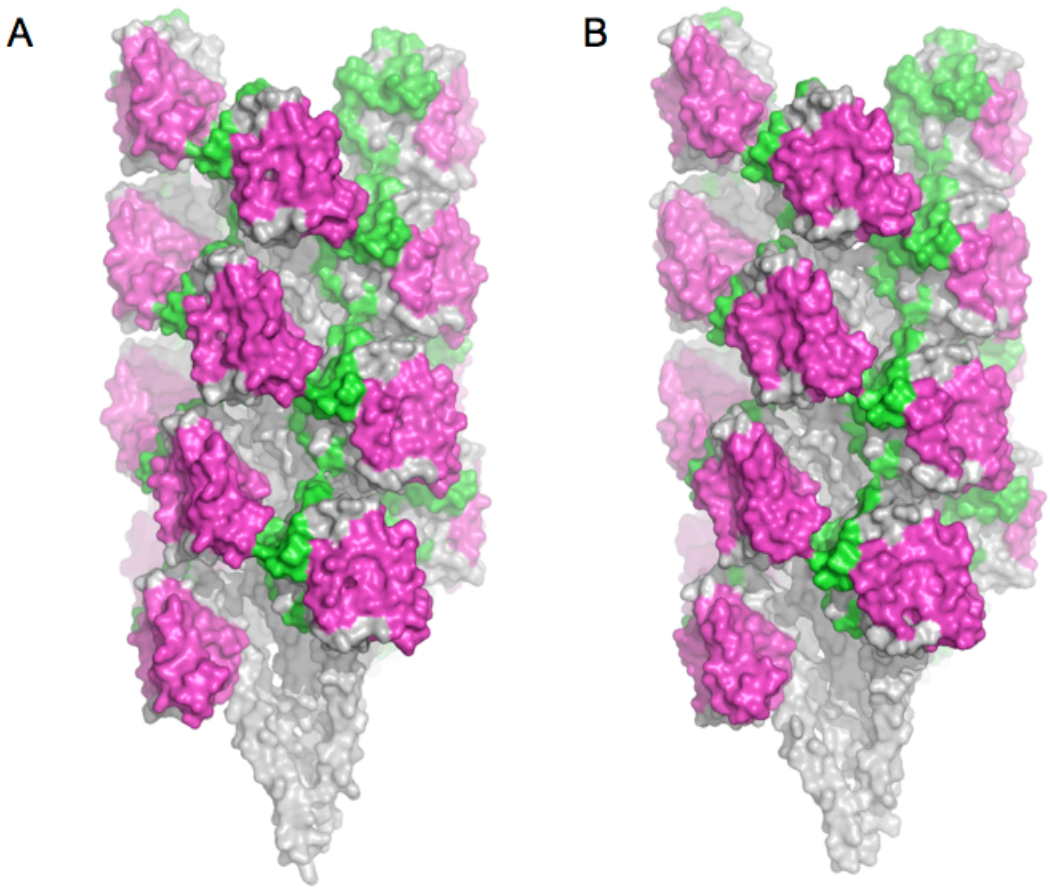

Figure 1.5 **Computational TCP model.** TCP model for (A) classical and (B) El Tor biotype. El Tor TCP model was generated by superposition of El Tor TcpA structure onto the classical TcpA subunits. Residues are colored as in Figure 1.4. Both filaments have large gaps in the surface that expose a segment of the N-terminal α-helix, and bulge of the C-terminal region of TcpA (magenta).

1.4. CTXϕ

CTXϕ is a *V. cholerae* specific filamentous, lysogenic bacteriophage that carries a single stranded 7 kb circular DNA genome encoding the cholera toxin A and B subunits, *ctxAB* (Waldor *et al*., 1996). CTXϕ infects *V. cholerae* by binding to TCP (Figure 1.6). The CTXϕ ssDNA genome is transported into the cytoplasm by an unknown mechanism (Figure 1.6). Within *V. cholerae* cells, CTXϕ can exist

either as a replicating plasmid (RF, replicative form of DNA), pCTX, or as a prophage integrated into the chromosome. CTXϕ DNA is generally found integrated at either one (El Tor biotype) or two (classical biotype) loci within the *V. cholerae* genome (Mekalanos *et al*., 1983; Pearson *et al*., 1993; Waldor *et al*., 1996). The CTXϕ genome carries the phage core region genes *zot*, *ace*, and *orfu*, which are thought to produce proteins needed for virion assembly and secretion. CTXϕ infection is a key event in the conversion of non-toxigenic *V. cholerae* strains into toxigenic strains as it introduces the cholera toxin genes, *ctxAB*, into the bacterial genome where they are then expressed along with *V. cholerae* gene products.

In El Tor strains, CTX prophage DNA is usually found in tandem arrays that also include a related genetic element, RS1. RS1 contains the genes that enable phage DNA replication and integration (*rstR*, *rstA*, and *rstB*) plus an additional gene of unknown function, *rstC* (Mekalanos *et al*., 1983; Waldor *et al*., 1997). Most analyses of the structure of CTX prophage arrays and of CTXϕ have used El Tor strains and virions derived from the El Tor biotype. Consequently, little is known about the structure of CTX prophage arrays in the classical biotype.

There are biotype-specific differences between the CTX prophage genomes from El Tor strains and the corresponding regions of the classical prophage (Kimsey *et al*. 1998). The prophages of El Tor strains yield infectious CTXϕ. In contrast, classical strains do not produce CTXϕ, although they contain CTX prophage integrated in the genome (Mekalanos *et al*. 1983; Kimsey *et al*.,

1998; Davis *et al*., 2000). However, classical strains such as O395 do produce a high titer of virions following infection of El Tor CTXϕ (Waldor et *al*., 1996). These data suggest that all of the proteins required for CTXϕ production can be generated from the prophages within the classical strains but they fail to produce the extra-chromosomal RF of the classical prophage DNA, pCTX. Instead of an RS1 followed by a CTX prophage, CTXϕ insertion sites in classical strains contain either a solitary prophage or a prophage array composed of two truncated, fused prophages. Neither of these arrangements is predicted to yield extrachromosomal CTXϕ DNA in classical biotypes (Davis *et al*., 2000).

V. cholerae produce relatively few CTXϕ compared to *E. coli* production of Ff phage. In the natural environment, sunlight appears to be the inducing agent of CTXϕ production. Exposure of cultures of CTXϕ lysogens to direct sunlight increased phage titers whereas other variables such as temperature, pH or salinity of the culture did not affect phage induction (Faruque *et al*., 2000). Induction of CTXϕ was not observed inside the intestine of the human host (Faruque *et al*., 1998). Transcription of the prophage genes is usually inhibited by the phage encoded repressor protein, RstR. RstR is synthesized and binds to the phage *rstA* promoter, preventing expression of all the downstream phage morphogenesis genes (Davis *et al*., 2002; Kimsey *et al*., 1998). RstR levels are reduced in response to the DNA damaging agent mitomycin (Davis *et al*., 2003) and UV from sunlight (Faruque *et al*., 2000).

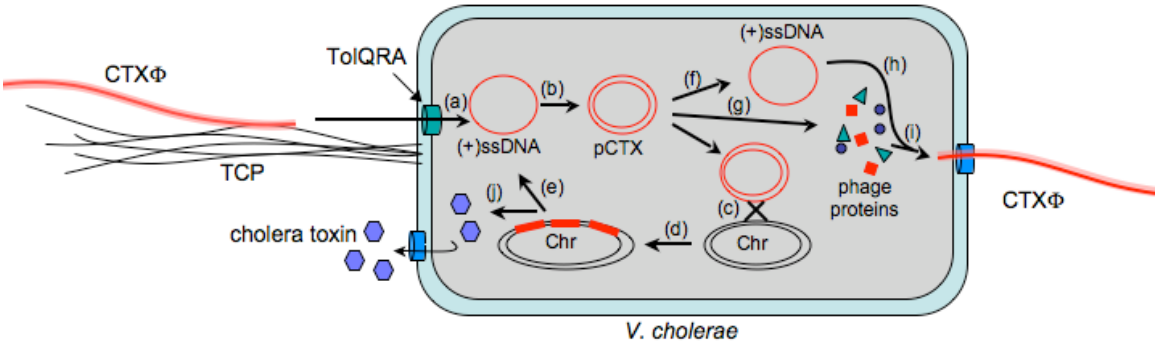

Figure 1.6 **CTXϕ infection of *V. cholerae*.** (a) CTXϕ infects *V. cholerae* by binding to TCP then to the inner membrane/periplasmic TolQRA complex. The phage ssDNA loses its protein coat and is transported into the cytoplasm. (b) The replicative or plasmid form of CTXϕ (pCTX) DNA is generated by replication of the ssDNA. (c) pCTX integrates site-specifically into *V. cholerae* chromosome. (d) pCTX usually integrates as tandem prophage. (e) CTX prophage serve as templates to generate extra-chromosomal (+)ssDNA. (f) (+)ssDNA is also generated off pCTX for packaging into new phage. (g) The phage coat and secretion proteins are expressed from pCTX. (h, i) The (+)ssDNA is packaged into phage particles at the inner membrane and secreted. (j) Cholera toxin subunits A and B are synthesized from *ctxAB* genes in the CTX prophage, assembled into holotoxin in the periplasm and secreted.

The open reading frames of the genes required for CTXϕ morphogenesis resemble those of the paradigmatic F-pilus specific filamentous phages of *E. coli* such as M13 (Ff phages). The genes that encode coat and secretion proteins for both CTXϕ and Ff phage are similar in size and arrangement within their respective genomes, although they have limited sequence homology (Figure 1.7).

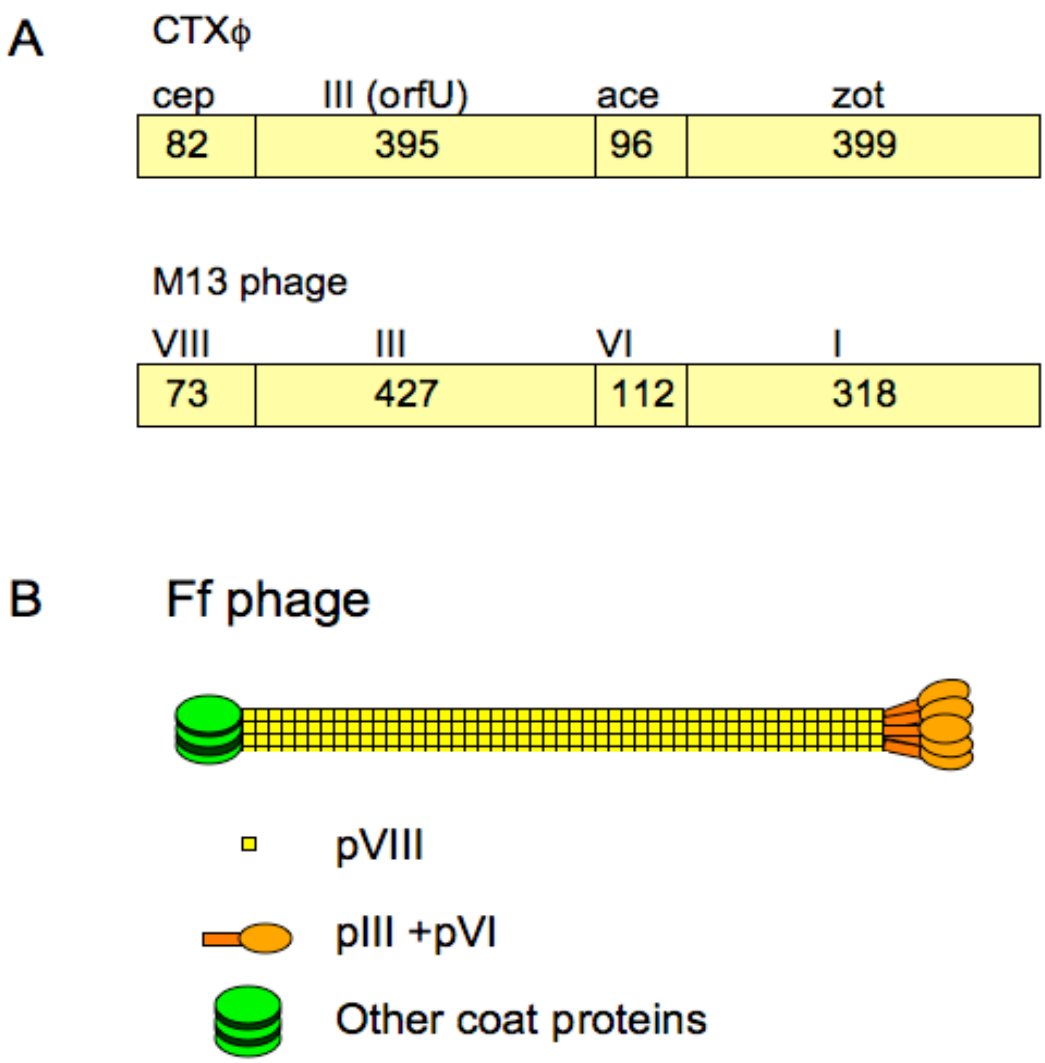

Figure 1.7 **Filamentous phage.** (A) Comparison of gene organization and size (in base pairs) for core structural proteins for CTXϕ and M13 phage (Ff phage). Adapted from Waldor *et al*. 1996. (B) Schematic representation of Ff phage. Adapted from Clackson *et al*. 2004.

The CTXϕ gene, *cep*, lies at the same site on the Ff genome as gene *VIII*, which encodes the major coat protein, pVIII. Like pVIII, Cep is a small protein (47 amino acids) and by analogy with pVIII, several thousand copies of Cep surround the ssDNA and form the hollow tube (Figure 1.7B). The four positively charged residues at the C-terminus of Cep are at the inner surface of the tube and

interact with the phosphates of the viral ssDNA. The gene product for *orfU* was recently renamed pIII from OrfU, because of its similarities with the minor coat protein pIII of Ff phage. In Ff phage, pIII is required for phage assembly and binding to the F-pilus. Waldor *et al*. (2003) introduced N-terminal fragments of CTXϕ pIII onto the Ff phage fd, and showed that these engineered coliphage, which are normally specific to *E. coli*, could now infect *V. cholerae*. They also showed that the inner membrane proteins TolQRA, which are required for Ff transfection into *E. coli*, are also required for the engineered coliphage transfection into *V. cholerae* (Waldor *et al*., 2003). Since TCP are the receptors for CTXϕ, these results suggest that the CTXϕ pIII mediates attachment to TCP. The processes by which virions infect *E. coli* and *V. cholerae* and are released from bacteria appear to be similar. However, Ff titers typically exceed CTXϕ titers by a dramatic margin, a 10,000-fold difference (Davis *et al*., 2003). This is partly due to the fact that the CTXϕ is maintained within the chromosome and the expression of its genes is restricted by the phage repressor RstR. Because of their repression, most cells in a population of *V. cholerae* do not give rise to CTXϕ. CTXϕ is also more dependent on host encoded proteins than are the coliphages, as chromosomal gene products mediate both chromosomal integration and secretion of CTXϕ.

To understand the molecular interactions between CTXϕ and *V. cholerae*, I examined the effects of point mutations in TcpA on phage uptake, and studied TCP:CTXϕ interactions by immuno-gold labelled TEM analysis.

1.5 Overview of objectives

Despite more than a century of study, cholera still poses challenges and surprises for us. Cholera remains a major health threat to large populations in the world in part because there is no effective vaccine against the disease. Understanding the molecular mechanism of the key virulence factor, the TCP should help to unravel the molecular pathogenesis of this deadly disease and may provide new insights towards the development of an effective vaccine. Also, what we learn with this system may apply to Type IV pili from other pathogens, as well as to the related Type II secretion system, which secretes toxins and hydrolytic enzymes in *V. cholerae* and other Gram-negative bacterial pathogens.

In this study I defined discrete regions of the pilin subunit that are directly involved in pilus assembly, pilus bundling, microcolony formation and CTXϕ interactions using structure-based, site-directed mutagenesis. The specific aims are as follows:

Aim 1: validating the pilus assembly model. In our filament models of TCP for the two *V. cholerae* biotypes, TcpA subunits are held together primarily by extensive hydrophobic interactions among the N-terminal α-helices. However, there is also a discrete interface between the $\alpha\beta$-loop of one subunit and a segment of the N-terminal α-helix of its neighbouring subunit. We hypothesized that this interface might be involved in pilus assembly. To test this, select residues in these regions were substituted and the effect of these replacements on pilus assembly was investigated.

Aim 2: investigating pilus:pilus interactions. To understand the molecular basis for pilus-mediated microcolony formation, I explored differences between TCP of *V. cholerae* classical and El Tor biotypes. We hypothesized that surface exposed, non-conserved residues between classical and El Tor TcpA mediate TCP:TCP interactions. To test this, residues in classical TcpA were substituted individually and in clusters for their respective residues in El Tor TcpA. The effects of these replacements were examined with emphasis on pilus:pilus interaction patterns.

Aim 3: investigating TCP:CTXϕ interactions. *V. cholerae* strains that do not produce TCP are not susceptible to CTXϕ infection when standard infection protocols are used, suggesting that TCP is the cell surface receptor for CTXϕ (Waldor *et al*., 1996; Kirn *et al*., 2000). Yet, this interaction has never been directly visualized. I sought to obtain the first microscopic evidence for TCP:CTXϕ interactions by employing immuno-gold labelling. In addition to TEM analysis, mutational analysis on TcpA subunit was completed in order to identify discrete regions involved in the interaction with CTXϕ. Since CTXϕ infects both classical and El Tor *V. cholerae,* I expected that the TCP residues involved in CTXϕ interactions are surface exposed and conserved between classical and El Tor biotypes. To test this, conserved residues in classical TcpA were replaced to alanine. Other TcpA replacements generated in Aim 2 were also examined for their effects on CTXϕ infection.

CHAPTER 2: MATERIALS AND METHODS

2.1 Bacterial strains

V. cholerae strains O395, C6706, RT4524, RT4340 and CL101, *E. coli* strain S17, plasmid pTK1 and anti-TcpA antibody were gifts from Ronald K. Taylor, Dartmouth Medical School. Details of bacterial strains are described in Table 1. *E. coli* strains were grown in Luria-Bertani (LB) broth at 37°C. *V. cholerae* strains grown under TCP-expressing conditions were grown in LB broth, pH 6.5, at 30°C for 16 hours. El Tor strain, C6706, was grown for four hours at 37°C in stationary tubes containing AKI media (1.5% Bacto-Pepton, 0.4% yeast extract, 0.3% $NaHCO_3$), followed by 12 hours at 30°C with rotation (Iwanaga *et al*., 1987; Medrano *et al*., 1999). All strains were stored at -80°C in LB containing 15% glycerol (v/v). Streptomycin (Sm) was used at a final concentration of 100 μg/mL, kanamycin (Kan) at 45 μg/mL, gentamicin (Gm) at 30 μg/mL, ampicillin (Amp) at 100 μg/mL and 5-bromo-4-chloro-3-indolyl β–D-galactopyranoside (X-gal) at 20 μg/mL.

Table 1 Bacterial strains

Bacteria	Description	Reference/Source
V. cholerae O395*	Wild type, classical (O1 classical strain)	Taylor *et al*. 1987
V. cholerae RT4236	Classical strain O395, lacking flagella	R.K. Taylor
V. cholerae RT4524	tcpA::*lacZ*	R.K. Taylor
V. cholerae RT4340	Wild type El Tor TCP on *V. cholerae* O395	R.K. Taylor
V. cholerae C6706	Wild type, El Tor	R.K. Taylor
V. cholerae ML 21	R26E	This study
V. cholerae ML 22	L76K	This study
V. cholerae ML 23	E83R	This study
V. cholerae ML 24	R26E/E83R	This study
V. cholerae LC1	A138E	This study
V. cholerae LC6	K187T	This study
V. cholerae LC7	A156D/E158A	This study
V. cholerae LC9	A138E/A156D/E158A	This study
V. cholerae LC10	A138E/A156D/E158A/K172A	This study
V. cholerae LC11	A138E/A156D/E158A/K187T	This study
V. cholerae LC12	A156D/E158A/K172A/D175N	This study
V. cholerae LC13	A138E/A156D/E158A/K172A/D175N	This study
V. cholerae LC15	A156D/E158A/K172A/D175N/K187T	This study
V. cholerae LC16	A138E/A156D/E158A/K172A/D175N/K187T	This study
V. cholerae ML9	D113A	This study
V. cholerae ML10	C120A	This study
V. cholerae ML12	D175N	This study
V. cholerae ML14	K172A/D175N	This study
V. cholerae ML15	A156D	This study
V. cholerae ML16	A138E/A156D/E158A/K172A/K187T	This study
V. cholerae ML17	E158A	This study
V. cholerae ML18	K172A	This study
V. cholerae ML25	LC16 with D156A	This study
V. cholerae ML28	D113G	This study
V. cholerae ML29	K85E	This study
V. cholerae ML30	K85A	This study
V. cholerae ML 2	V161A	This study
V. cholerae ML 8	T159A	This study
V. cholerae ML 11	A102D	This study
V. cholerae RT4225	H181A	Kirn *et al*., 2000
V. cholerae CL101	pCTX-Kanϕ	Kirn *et al*., 2000
E. coli S17	λpir	Skorupski *et al*. 1996
E. coli RT4024	*E. coli* S17 with pTK1	R.K. Taylor
E. coli KSK580	X90 with pMT5: has *toxT* gene under control of *lac* promoter (IPTG inducible)	DiRita *et al*. 1996
E. coli KSK575	MM294 with pRK2013, a helper plasmid for pMT5	Figurski *et al*. 1979
*All *V. cholerae* TcpA mutants were derived from O395, classical biotype. All mutants contain pMT5		

2.2 Generation and isolation of *tcpA* mutants

Since the methods and expression systems that were obtained from Ronald K. Taylor, Dartmouth Medical School, use classical *V. cholerae,* and autoagglutination is most evident in this biotype, I made mutations in this system.

2.2.1 Site-directed mutagenesis

Complementary, mutagenic primers (Table A1) were designed to generate missense mutations in pTK1, by QuickChange mutagenesis (Stratagene). pTK1 is a pKAS32 suicide vector containing genes encoding wild type *tcpA* and β-lactamase, which confers ampicillin resistance on its host (Kirn *et al*., 2000). After polymerase chain reaction (PCR), amplified pTK1 containing the mutated *tcpA* gene (*tcpA**), was incubated with DpnI to cleave the methylated parental plasmid at GA^{m}TC sites (Figure 2.1). One μL of this product was used to transform *E. coli* S17 cells by electroporation. Colonies containing pTK1-*tcpA** were selected on LB-agar-Amp plates and plasmid was purified using a plasmid miniprep kit (QIAGEN). Purified plasmids were sequenced to confirm the desired mutation (Table A2).

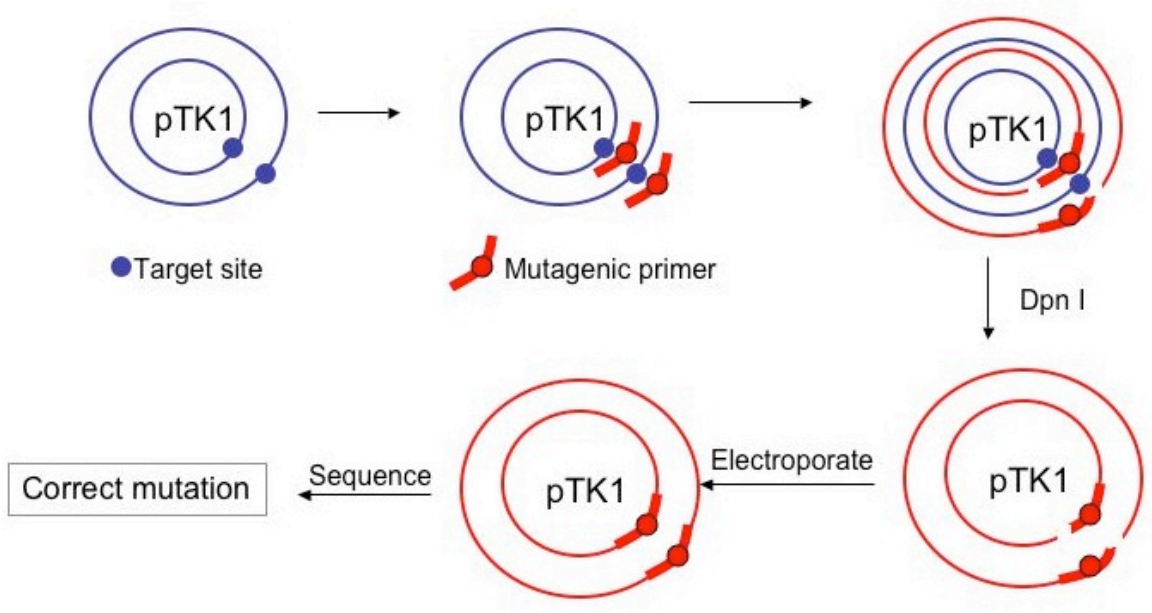

Figure 2.1 **Site directed mutagenesis.** A point mutation was introduced into the *tcpA* gene on pTK1 using mutagenic primers. The parental strain of pTK1 was cleaved with Dpn1. Newly generated pTK1 carrying the desired *tcpA** mutation was electroporated into *E. coli* S17 cells and pTK1 was sequenced to confirm the correct mutation.

2.2.2 Allelic exchange

E. coli S17 cells carrying the correct sequence of mutated *tcpA** on pTK1 plasmid were mated with *V. cholerae* classical strain RT4524. *V. cholerae* RT4524 has the *tcpA* gene disrupted by a *lacZ* gene fragment and it is gentamicin and streptomycin resistant (Gm^R, Sm^R). Gm^R is conferred by plasmid pMin1 in RT4524, and *V. cholerae* are naturally Sm^R due to a mutation in the S12 protein, which makes it unable to bind Sm. Mating was carried out according to Maloy *et al*. (1996). *E. coli* S17 cells were streaked in a crosshatch pattern onto parallel streaks of *V. cholerae* RT4524 cells on LB agar. After incubating 24 hours at 37°C, a swipe of cells for each crosshatch was streaked onto Amp-Gm-

LB plates and grown overnight at 37°C to select for *V. cholerae* transconjugants. The pTK1 plasmid is a suicide vector that requires the pi protein to replicate (Skorupski *et al*., 1996). pTK1 can replicate independently in *E. coli* S17 cells that produce pi proteins, but cannot replicate independently in *V. cholerae* RT4524, which lacks the pi protein. Thus, only *V. cholerae* cells that have the pTK1 plasmid integrated into the host genome (transconjugants) will be ampicillin resistant (Amp^R). Gm was included in the medium to select for *V. cholerae* cells over *E. coli* cells (Figure 2.2). The transconjugants were also streptomycin sensitive (Sm^S) due to the presence of the *rpsL* gene on pTK1. *rpsL* encodes ribosomal protein S12, which is required for translation. Wild type S12 protein binds to streptomycin and has a dominant effect, making the *Vibrio* transconjugants Sm^S. The first homologous recombination event involves integration of pTK1 plasmid into the *V. cholerae* genome by a single crossover at a region of homology between *tcpA** and its 5' and 3' flanking regions (fl1 and fl2, respectively) on the plasmid and *tcpA* and its flanking regions on the *V. cholerae* Chromosome 1. A second homologous recombination occurs between the two *tcpA* genes, leaving only one copy of the gene on the chromosome, either the mutated copy or the original copy containing the *lacZ* gene fragment. Cells in which the pTK1 plasmid has been excised will now be Amp^S, Sm^R and Gm^R. For screening purposes, *V. cholerae* RT4524 contains a *lacZ* gene inserted into the *tcpA* gene. This strain produces β-galactosidase, which hydrolyzes 5-bromo-4-choloro-3-indolyl-β-D-galactoside (X-gal), turning colonies dark blue on X-gal-agar plates. In cases in which the *tcpA-lacZ* gene is replaced with the mutated

*tcpA** during excision of the plasmid, the colonies appear light blue on X-gal-agar plates as opposed to dark blue if β-galactoside is present. Light blue colonies were picked from the transconjugants grown on Sm-Gm-Xgal plates at 30°C for two days. Colors of the colonies were confirmed again by plating the selected colonies on Sm-Gm-X-gal plates and incubating them for two more days at 30°C. Colors of the mutant colonies were compared to *V. cholerae* RT4524 strain with the *lacZ* gene, which forms a dark blue colony and the *V. cholerae* O395 strain lacking the *lacZ* gene, which forms a light blue colony. Light blue colonies of the mutant strains were plated on Amp to confirm the excision of pTK1. Genomic DNA was purified from these mutant strains (Puregene DNA purification system) and PCR was used to amplify the mutated *tcpA** gene. The correct size of PCR product was confirmed by 1% agarose gel electrophoresis after which the DNA band was excised from the agarose gel, and sequenced to confirm the mutation (NAPS, UBC). Clones with the correct mutations were grown for a few generations at 42°C to cure the plasmid, pMIN1, which confers Gm^R.

To each *V. cholerae* mutant strain the pMT5 plasmid was introduced. pMT5 carries the gene for the transcriptional activator ToxT under the control of an inducible promoter. ToxT up-regulates transcription of the TCP operon and thus allows overexpression of TcpA.

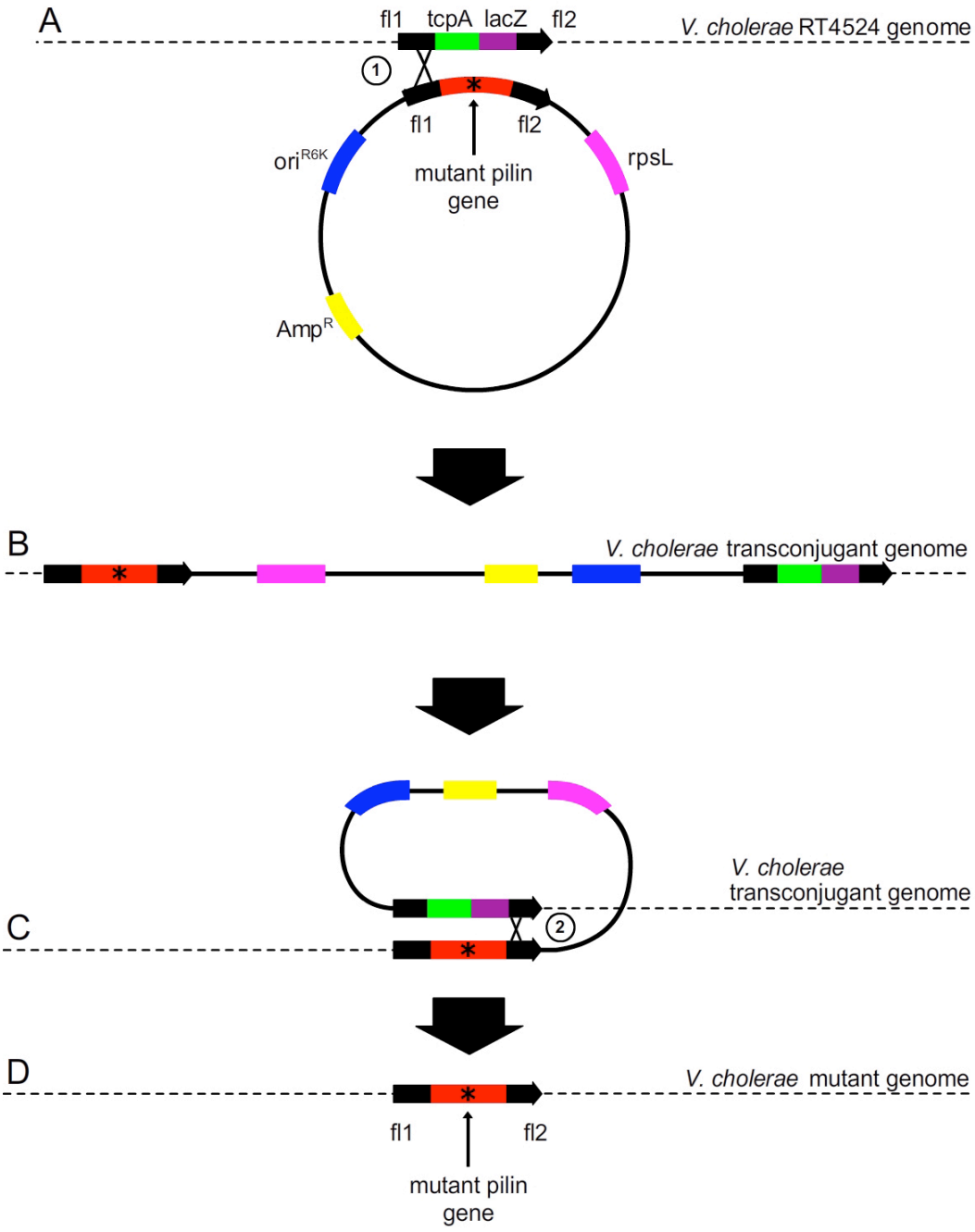

Figure 2.2 **Allelic exchange.** (A) First homologous recombination occurs at the homologous sequence between pTK1 carrying *tcpA** mutation and *V. cholerae* RT4524 genome producing (B) transconjugants. (C) Second homologous recombination occurs at a region of homology (D) leaving mutation* on *V. cholerae* genome. Only one possible result of homologous recombination is shown.

2.3 Screening of *tcpA* mutants

2.3.1 Autoagglutination

A facile *in vitro* assay for the expression of functional TCP on *V. cholerae* surfaces is an autoagglutination test. Autoagglutination *in vitro* has been correlated with microcolony formation and colonization of the small intestine in an infant mouse model (Kirn *et al*., 2000). *V. cholerae* grown under TCP-expressing conditions will clump together, autoagglutinate, and fall to the bottom of the tube after overnight growth if they express functional TCP. Strains that do not assemble TCP, or have weak TCP:TCP interactions, do not autoagglutinate and remain suspended in the culture. Two mL cultures of each strain were grown under TCP-expressing conditions. Autoagglutination was scored visually, relative to the wild type classical *V. cholerae* strain, O395 (Figure 2.3).

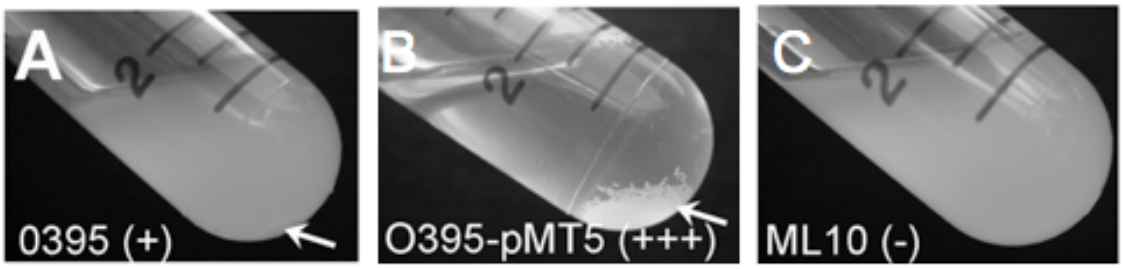

Figure 2.3 ***In vitro*** **microcolony formation, autoagglutination.** Autoagglutination of overnight *V. cholerae* cultures grown under TCP-expressing conditions. (A) classical biotype O395, (B) O395-pMT5, and (C) ML10-pMT5 (ML10 has a C120A mutation in TcpA, which abrogates pilin expression). O395-pMT5 show complete autoagglutination (+++), where the cells fall out of the solution in large grainy aggregates, leaving a clear supernatant. O395 without pMT5 shows partial autoagglutination (+), as indicated by the clump of aggregated cells (arrow), whereas ML10 shows no autoagglutination (-).

2.3.2 SDS-PAGE and immunoblotting to assess pilin expression and pilus assembly

Mutations in the *tcpA* gene may abrogate autoagglutination at a number of levels: by disrupting *tcpA* folding, pilus assembly or pilus surface chemistry. To ensure that the mutated pilin subunits are expressed and folded properly, sodium dodecyl sulfate polyacrylamide gel electrophoresis (SDS-PAGE) and immunoblotting was performed on whole cell cultures grown overnight under pilus-expressing conditions. To test whether TCP were assembled on the cell surface, TCP were sheared from cells by homogenization of the overnight cultures. The supernatants from the homogenates were analyzed by SDS-PAGE and immunoblot. An Ultra-Turrax T8.01 disperser was used to physically shear the pili from the cells. Cell densities of the strains were normalized based on optical density measurements. Pilin production was accessed by running 24 μl of normalized whole cell cultures on SDS-PAGE. After electrophoresis, gels were either Coomassie-stained or transferred to PVDF membrane and immunoblotted using an antibody directed against a peptide in the C-terminus of TcpA (TcpA6, Taylor *et al*., 2004). Pilus expression was assessed by immunoblotting 24 μL of normalized cell homogenates containing sheared pili.

2.3.3 Transmission electron microscopy imaging to assess TCP morphology and bundling

V. cholerae cells were grown overnight in 2-mL cultures under pilus-expressing conditions. Five μL of overnight culture was applied to carbon-coated copper grids. After five min, the culture was wicked off and the grids were washed with two drops of phosphate-buffered saline (PBS, 137 mM sodium

chloride, 2.7 mM potassium chloride and 10 mM phosphate buffer) then stained with either 1% phosphotungstic acid (PTA) or 1% ammonium molybdate. Grids were imaged by transmission electron microscopy (TEM) in the FEI Tecnai F20 at 20,000-42,000X magnifications. Mutations that result in normal TCP morphology but altered autoagglutination and bundling characteristics indicate residues involved in pilus:pilus interactions.

2.3.4 CTXϕ infection

V. cholerae CL101 classical biotype carries CTX-Kanϕ which has replaced the *ctxAB* gene with the marker for kanamycin resistance (Waldor *et al*.,1996). This CTX-Kanϕ is originally from El Tor strain and it replicates as a plasmid, pCTX, in classical *V. cholerae* CL101 (Waldor *et al*., 1996). After overnight growth under pilus-expressing conditions, *V. cholerae* CL101 cells were pelleted and the supernatant was filtered on 0.2-μm filter (Nalgen) to remove residual cells. Filtered supernatant containing CTX-Kanϕ was mixed with overnight cultures of *V. cholerae* cells carrying *tcpA* mutations in a 1:5 ratio (v/v). This mixture was incubated at room temperature for 30 min, then serial dilutions were plated on Kan-LB-agar plates. Additionally, *V. cholerae* strains being tested were plated on Sm-LB-agar plates to calculate the number of input bacteria. Transduction frequency was calculated as the ratio of Kan^R test strain transductants (colony forming unit, cfu) to the number of input cfu. Transduction efficiency was reported as the ratio of transduction frequency of the test strain to the transduction frequency of the wild type strain, O395.

2.4 Immuno-gold labelling

2.4.1 CTXϕ-Cep antibody production

Synthetic peptide and antibody were produced by Pacific Immunology California, USA. CTXϕ antibody was raised in New Zealand White rabbits against a synthetic peptide comprising amino acids 36-DAGLVTEVTKTLGTSKDT-53 in the Cep protein. Cysteine was added to the N-terminus and the peptide was conjugated to a carrier protein, keyhole limpet hemocyanin.

2.4.2 Purification of CTXϕ for TEM imaging

2.4.2.1 Expressing CTX-Kanϕ in flagella-minus *V. cholerae* strain

V. cholerae strain RT4236, which lacks flagella was infected with the cleared culture supernatant of CL101 cells to introduce the CTX-Kanϕ.

2.4.2.2 Large scale purification of CTXϕ for TEM imaging.

One litre of *V. cholerae* RT4236-CTX-Kanϕ culture was grown overnight for 20 hours in pilus non-expressing conditions (LB pH 8.5, 37°C). Cells were centrifuged and supernatant was filtered on 0.2-μm filter (Nalgene) to remove residual cells. Filtered supernatant was mixed with 0.15 volume of PEG 8000/NaCl (16.7%/3.3M). The mixture was incubated at 4°C overnight and then centrifuged for 40 min at 10,000 rpm to pellet the phage. The phage pellet was resuspended in PBS and residual PEG/NaCl was dialysed out.

2.4.3 TCP purification for TEM imaging

TCP used for imaging TCP:CTXϕ interactions have a change in the TcpA subunit, H181A, which causes them to be shed into the culture supernatant, allowing large-scale purification. TCP^{H181A} filaments from whole cell culture resemble wild type TCP by negative stain TEM, both in terms of pilus morphology and pilus:pilus interactions (Li *et al*., 2008). Importantly, H181A mutants transduce phage at wild type levels (Kirn *et al*., 2000), indicating that TCP^{H181A} interacts with CTXϕ. One litre of *V. cholerae* RT4225 (H181A) was grown under pilus-expressing conditions. After overnight growth, the culture was centrifuged at 5000*xg* for 15 min to remove the cells. The cleared supernatant was mixed with 10% ammonium sulfate (w/v) for two hours on ice, centrifuged at 10,000*xg* for 30 min to remove the insoluble fraction. The supernatant was then mixed with 30% ammonium sulfate to precipitate the pili, which were separated from the supernatant by centrifugation at 10,000*xg* for 30 min. Residual ammonium sulfate was removed by dialysis.

2.4.4 Immuno-gold labelling

2.4.4.1 Biotinylation of TCP for imaging

Five mM Sulfo-NHS-LC-Biotin (Pierce, Thermo Fisher Scientific) was dissolved in water immediately before use. A 20-molar excess of biotin was mixed with purified TCP^{H181A} for two hours on ice to biotinylate TCP^{H181A}. Residual biotin was removed by dialysis.

2.4.4.2 Preparation of TEM grids for immuo-gold labelling.

For single labelling, either 15 μL of biotinylated pili or purified CTXϕ was placed on a nickel grid for 15 min at room temperature. The grid was washed with four consecutive drops of Tris buffered saline containing Tween (TBST, 25 mM Tris, pH 7.4, 25 mM sodium chloride, 2.7 mM potassium chloride, 0.05% Tween-20, v/v), then blocked with 1% w/v bovine serum albumin in TBST (1% BTT) for 30 min. For biotinylated pili, 10 μL goat anti-biotin antibody conjugated to 20-nm gold particles (Ted Pella) was applied to the grid for 30 min. For CTXϕ, 10 μL 320 nM rabbit anti-Cep antibody (Pacific Immunology) was applied to the grid for one hour, followed by four TBST one-drop washes. Ten μL of a 1/10 dilution of goat anti-rabbit antibody conjugated to 10-nm gold particles (Ted Pella) was then applied to the grid for 30 min. The grid was washed four times with TBST then stained with either 1% PTA or 1% ammonium molybdate.

For double labelling (Figure 2.4), biotinylated pili were mixed with CTXϕ for five min in an Eppendorf tube then applied to a nickel grid for 10 min. The grid was blocked with 1% BTT for 30 min then goat anti-biotin antibody conjugated to 20-nm gold particles was applied to the grid for 30 min. The grid was washed four times with TBST, then 320 nM of rabbit anti-Cep antibody was applied to the grid for one hour followed by four TBST washes. Then goat anti-rabbit antibody conjugated to 10-nm gold particles was applied for 30 min on the grids. Following four TBST washes, the grid was stained with either 1% PTA or 1% ammonium molybdate.

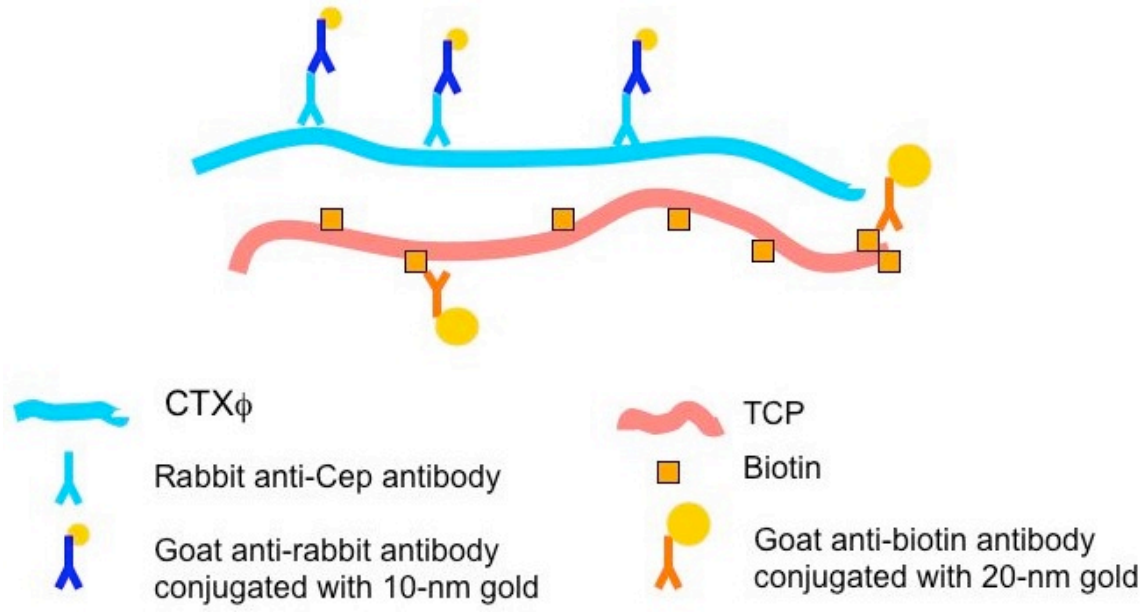

Figure2.4 **Immuno-gold labelling.** Biotinylated TCP^{H181A} and CTXϕ were mixed. Goat anti-biotin antibody conjugated with 20-nm gold particles label TCP^{H181A}. Goat anti-rabbit antibody conjugated with 10-nm gold particles label CTXϕ. Different sized gold particles allow distinction between TCP^{H181A} and CTXϕ by TEM.

2.5 Figure preparation

Molecule structure figures were prepared using PyMOL (http://www.pymol.org).

CHAPTER 3: PILUS ASSEMBLY

3.1 Introduction

TCP is assembled from multiple copies of its structural protein, TcpA. The molecular events that lead to polymerization of TcpA subunits to form filaments are poorly understood.

Pilin subunits are synthesized in the cytosol and transported across the inner membrane and remain anchored by their α1N region (Figure 1.4; Kaufman *et al*., 1993; Strom *et al*., 1993; Freitag *et al*., 1995). The 25-residue leader sequence is removed by the pilin peptidase, TcpJ, on the cytoplasmic face (Kaufman *et al*., 1991). The globular C-terminal domain folds in the periplasm, and a disulfide bond between residues C120 and C186 is formed by an oxidoreductase enzyme (Peek *et al*., 1992; Zhang *et al*., 1996). Pilus assembly requires a hexameric ATPase that associates with the cytoplasmic side of the inner membrane, and the presence of a GspF family integral inner membrane protein, IMP (Crowther *et al*., 2004; Tripathi *et al*., 2007; Collins *et al*., 2007). The molecular events that occur to link ATP hydrolysis and pilin subunit polymerization are unknown.

We hypothesize that the IMP operates like a piston, transmitting a conformational change of the ATPase subunit induced by ATP hydrolysis to extrude the pilus filament into the periplasm (Figure 3.1). This motion would occur each time a new pilin subunit docks onto the base of the growing filament.

The extrusion would open a gap large enough for a new subunit to dock and the filament would again be driven outward by an ATP hydrolysis event at another ATPase subunit in the hexameric ring and a corresponding piston stroke of another IMP. The subunit docking, ATP hydrolysis and piston stroke cycle would repeat, iteratively adding subunits around the base of the filament. Each subunit would be locked into the growing filament by the extrusion step, which would extract it from the inner membrane, to be held in place by hydrophobic interactions among the pilus subunits. Examination of TCP filament model suggested that chemical complementarity between pilin subunits might be involved in initiating pilus assembly. We hypothesize that the pilin subunits are attracted to the growing pilus filament in part because of complementarity between a conserved, negatively charged Glu5 side chain and the positively charged N-terminal residue of the subunit, both of which reside in the hydrophobic lipid bilayer. Additional chemical complementarity between discrete regions of the globular domains, or the globular domain and the N-terminal α-helix are expected to help dock the pilin subunits into the filament. The docked subunits would be stabilized by hydrophobic interactions between the neighbouring pilin subunits.

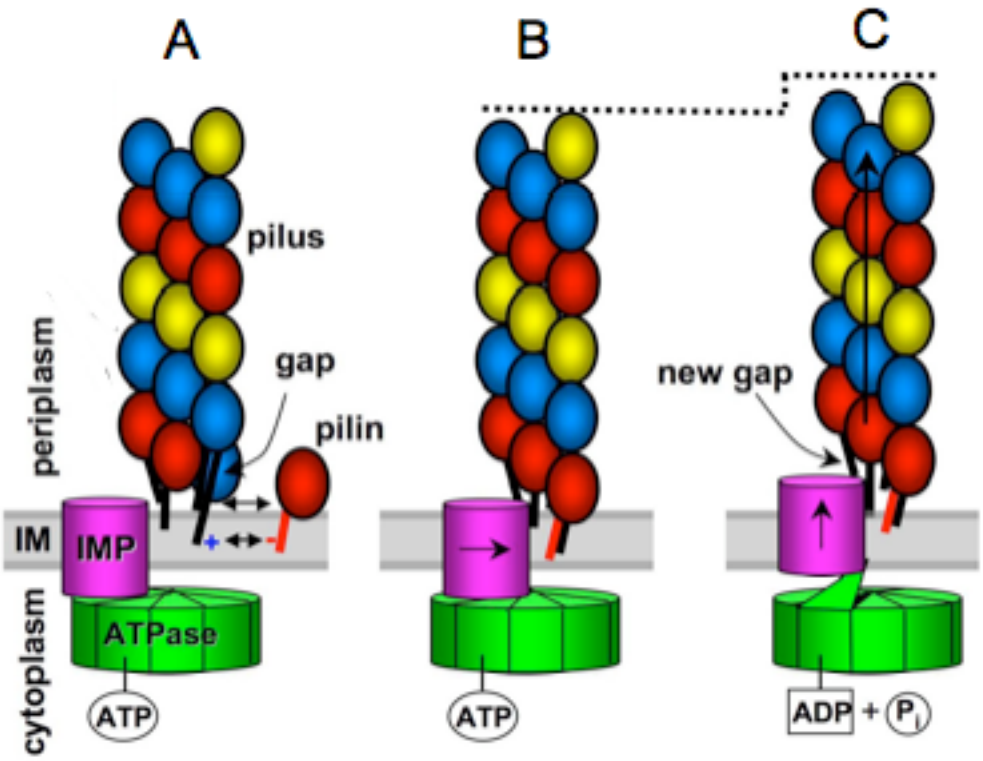

Figure 3.1 **Pilus assembly model.** (A) A pilin subunit docks into a gap at the base of the filament by electrostatic interactions between pilin subunits. (B) The integral inner membrane protein (IMP) binds to the docked pilin and its neighbouring subunits via their N-terminal α-helices. (C) ATP hydrolysis of ATPase induces a conformational change, which is transduced to its associated IMP. This conformational change at the ATPase drives the IMP a short distance through the membrane in a piston-like movement, extruding the pilus filament 8-10 Å into the periplasm. The outward movement of the filament opens up a new gap for docking of another pilin subunit. Diffusion of ADP out of the ATPase active site relaxes the ATPase subunit and allows the IMP to collapse back into the inner membrane. Courtesy of L. Craig.

The TCP model shows that TcpA subunits are held together almost entirely by interactions among the N-terminal α-helices, which form a tightly packed hydrophobic core in the filament (Figure 3.2). In addition to the hydrophobic interactions between the N-terminal α-helices, there is a small interface between the $\alpha\beta$-loop of one subunit and α1N of a neighbouring subunit (Figure 3.2), whereby a positively charged arginine (Arg26) is positioned to form

a stabilizing salt bridge with a negatively-charged glutamate (Glu83). This interaction may be important in TCP assembly and/or stabilization of the TCP filament. To test this hypothesis, I mutated residues at the putative α1N:αβ-loop interface by site-directed mutagenesis and allelic exchange.

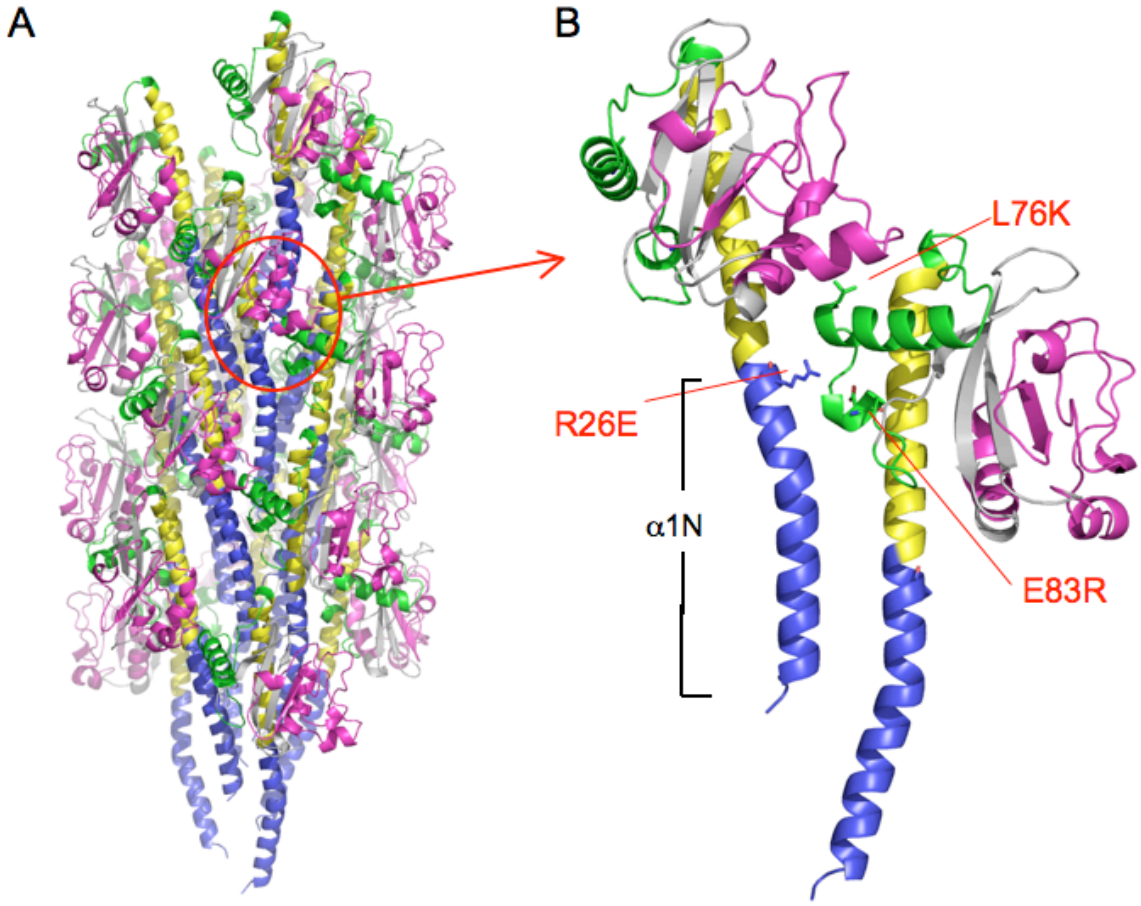

Figure 3.2 **Pilin:pilin interactions in the TCP filament.** (A) Ribbon representation of the computational TCP filament model. TcpA subunits are held together by extensive interactions among the N-terminal α-helices (α1N in blue, α1C in yellow). (B) Two adjacent subunits from the computational model shows residues (presented in sticks) that are likely to be involved in pilin:pilin interactions. D-region (bulge) is colored in magenta and αβ-loop is in green.

An understanding of the molecular interactions between the pilin subunits in the pilus filament can contribute to our understanding of the pilus assembly mechanism and the driving forces behind the translocation of pilin subunits from the stable inner membrane to an assembling pilus filament.

3.2 Results

The TCP filament model shows Arg26 in α1N could form an intermolecular salt bridge with Glu83 on the $\alpha\beta$-loop of a neighbouring subunit (Figure 3.2). To test the involvement of these two charged residues in filament assembly, Arg26 was mutated to Glu and Glu83 was mutated to Arg, both individually and as a double mutation, and the effects of these mutations on pilus assembly were examined. Each residue was mutated to its opposite charge to produce a more dramatic effect than a more conventional alanine mutation would produce. Because the subunit:subunit interactions are so extensive along the N-terminal α-helices, mutation of a charged residue to Ala at the smaller α1N:$\alpha\beta$-loop interface might not be sufficient to disrupt pilus assembly. Substitutions were made by site-directed mutagenesis of the classical *tcpA* gene on pTK1. This gene was then introduced by allelic exchange into recipient strain RT4524, a classical *V. cholerae* strain carrying a *lacZ* gene fragment in the *tcpA* gene for screening purposes. The ML7 strain was included as a positive control in which the *tcpA-lacZ* gene fusion of RT4524 was replaced with the wild type classical *tcpA* by allelic exchange. No substantial differences were observed between pilus levels or pilus morphology for O395 and ML7 as assessed by immunoblot

and TEM (data not shown). Strain ML10, which has a C120A mutation that abrogates pilin production, was included as a negative control.

V. cholerae mutants were tested for: (i) their ability to produce pilin protein, as assessed by immunoblot analysis of whole cell culture using anti-TcpA antibody; and (ii) their ability to assemble TCP, as assessed by TEM analysis, and by the presence of TcpA protein in the supernatant of homogenized cells. Additionally, CTXϕ infection was used to confirm the presence of assembled TCP, as CTXϕ requires TCP to infect *V. cholerae* cells. Pilin protein was observed at wild type levels in whole cell cultures for both *V. cholerae* mutants, R26E and E83R (Figure 3.3), indicating that these mutations do not disrupt the pilin fold. This is in contrast to a folding mutation, Cys120 to Ala, which disrupts the conserved Cys120-Cys186 disulfide bridge, and results in the absence of pilin protein detected by the immunoblot (Figure 3.3).

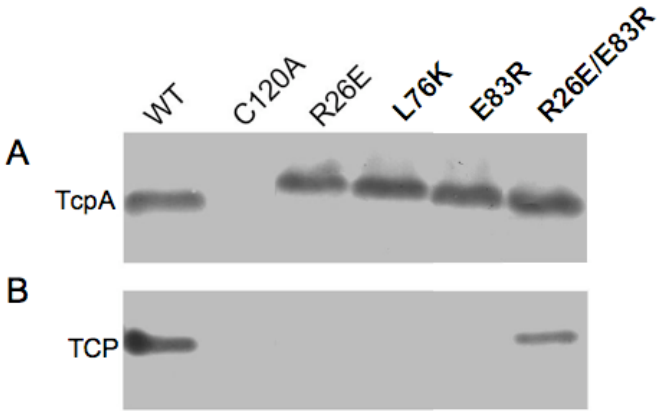

Figure 3.3 Immunoblot analysis of pilin expression and pilus assembly for TcpA mutants. Immunoblot showing (A) pilin subunit expression in whole cell lysates and (B) pilus assembly indicated by the presence of pilin protein in sheared cell homogenates. WT refers to wild type *V. cholerae* O395, classical biotype.

To test pilus expression, intact pili were sheared from cells by homogenization, and the homogenized cell supernatants were analyzed by SDS-PAGE and immunoblotting. TcpA was not detected in sheared cell supernatant for the R26E mutant, but a small amount of TcpA was detected in the E83R mutant (Figure 3.3). TCP production was also tested by TEM analysis (Figure 3.4). TCP was not observed for the R26E mutant. However, a few TCP filaments were observed by TEM in the E83R mutant, confirming low levels of pilus production by this strain (Figure. 3.4). To confirm the presence of assembled pilus, these mutants were infected with CTXϕ. CTXϕ failed to infect the R26E mutant. The E83R mutant was infected at a low level, 100 fold less, compared to the wild type, O395. These results confirmed the lack of assembled pili in the R26E mutant and low levels of pili in the E83R mutant.

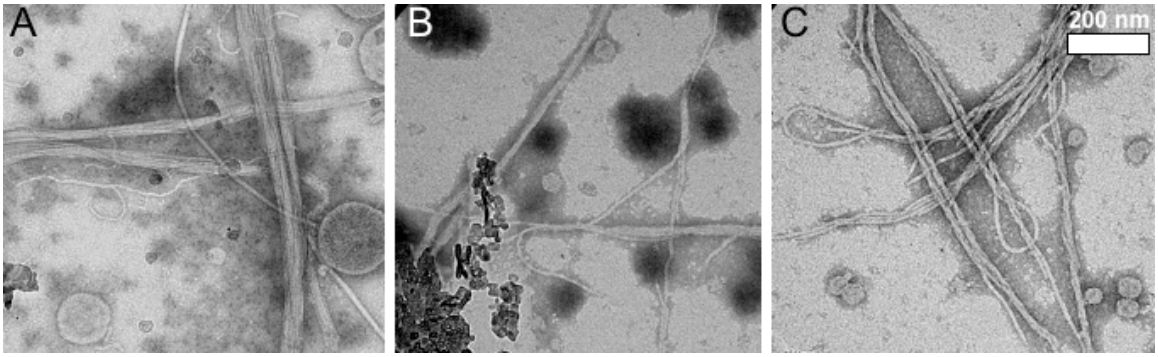

Figure 3.4 **TEM images**. (A) Wild type, O395. (B) E83R mutant. (C) R26E/E83R double mutant. Scale bar for all panels, 200 nm.

The dramatic reduction in pilus expression for the R26E and E83R mutants clearly demonstrates a role for Arg26 and Glu83 in pilus assembly. Importantly, the R26E and E83R double mutant partially rescued pilus assembly,

producing about half the level of wild type TCP (Figure 3.3). This supports a direct interaction between Arg26 and Glu83, as predicted by the computational filament model. To further test the role of the α1N:αβ-loop interaction interface, Leu76, which is centrally located in this interface, was changed to Lys. Bacteria carrying this mutation produced pilin but not pili, as detected by immunoblot (Figure 3.3), TEM studies (data not shown) and its inability to be infected by CTXϕ. This result implicates Leu76 in filament assembly, demonstrating that the α1N:αβ-loop interface involves both hydrophobic and ionic interactions. The results in this section are reported in mutagenesis section of Li *et al*. (2008).

3.3 Discussion

Site directed mutagenesis of *tcpA* was used to characterize the nature of the pilus assembly. Mutations at the small interface between α1N:αβ-loop had a dramatic effect on pilus assembly, confirming the involvement of this interface in pilus assembly. However, if the R26:E83 salt bridge was essential for pilus assembly, no TCP filaments should have been observed for either mutant. This interface is relatively small compared to the extensive multiple interfaces formed among the N-terminal α-helices (Figure 3.2), so it is in fact remarkable that single mutations, such as R26E, L76K, and E83R, have such dramatic effects on pilus assembly. Thus, we speculate that the α1N:αβ-loop interfaces are not actually required for the pilus stability, but are instead involved in initiating the addition of each subunit to the growing pilus. During pilus biogenesis, pilin subunits translocate across the inner membrane. These subunits are likely to remain anchored in this membrane via their hydrophobic α1N helices prior to being

incorporated into a growing pilus filament (Figure 3.1A). From the mutational analysis in this study, we speculate that electrostatic interactions between subunits are part of the driving force that translocates pilin subunits from their seemingly stable anchorage in the inner membrane to an assembling pilus filament. Electrostatic interactions such as the charge complementarity between Arg26 and Glu83 may be important for initiating pilus assembly. In addition, since no pili were produced by the L76K mutant, it is clear that overall chemical complementarity, and not just electrostatic complementarity at this small interface, is important for the assembly process. In the absence of complementarity between these two surfaces, pilus assembly may occur but is much less efficient, explaining the dramatic reduction in pilus expression for the α1N:$\alpha\beta$-loop interface mutants. We speculate that once the docked pilin subunit is extruded into the periplasm, it is stabilized by the extensive hydrophobic interactions among the N-terminal α-helices, which then firmly anchor the subunits in place.

CHAPTER 4: PILUS:PILUS INTERACTIONS

4.1 Introduction

TCP mediated microcolony formation is not well understood but appears to require very precise interactions. Kirn *et al*. showed that single amino acid changes in the *V. cholerae* TCP can alter pilus:pilus interactions, as assessed by *in vitro* microcolony formation, autoagglutination, and colonization of the infant mouse (Kirn *et al*., 2000). They also showed that autoagglutination *in vitro* correlates well with the colonization of the infant mouse small intestine *in vivo*, indicating autoagglutination as a reliable predictor of *in vitro* colonization efficiency.

Both biotypes, classical and El Tor, require TCP to colonize human and murine intestines. TcpA from the two biotypes, classical and El Tor, have 81% amino acid sequence identity (Figure 4.1) and have virtually identical protein folds, as determined by their x-ray crystal structures (Figure 4.2, Craig *et al*., 2003, unpublished data).

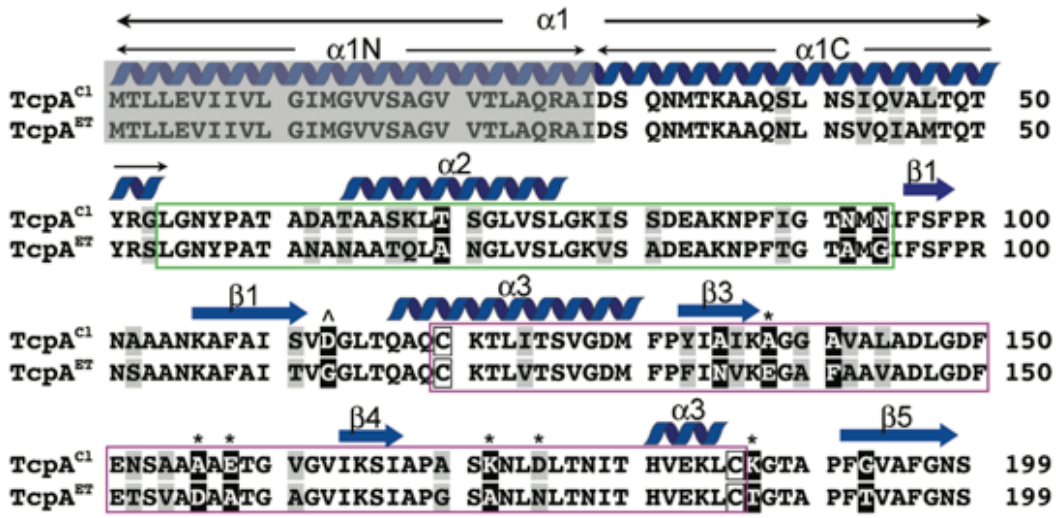

Figure 4.1 **Comparison of the amino acid sequences for classical and El Tor TcpA.** Amino acid sequence alignment for mature TcpA proteins from classical *V. cholerae* O395 and El Tor strain C6706. The secondary structure for TcpA from classical strain is indicated above the sequence. The αβ-loop is boxed in green and the D-region is boxed in magenta. Crystal structures lack α1N (residues 1-28, shaded grey). Conserved amino acid sequences between the two biotypes are highlighted in grey and non-conserved changes are shown in black with white letters. An asterisk (*) above the residue indicates classical-to-El Tor mutations located on the D-region surface patch, and the carat (^) for residue 113 indicates a classical-to-El Tor mutation located in the cavity between the subunits in the TCP filament. The 25-residue leader sequence, which is removed prior to incorporation of the pilin subunits into the pilus filaments, is not shown.

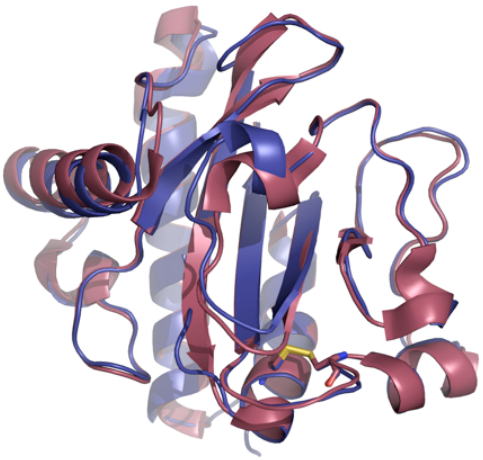

Figure 4.2 **Superposition of classical and El Tor TcpA crystal structures**. N-terminally truncated TcpA crystal structures from classical (red) and El Tor (blue) strains. Conserved disulfide bridges are represented as sticks.

Despite these similarities in amino acid sequence and protein fold, we observed a dramatic differences in pilus:pilus interactions. By TEM, TCP from both biotypes have similar morphologies, being long, relatively straight filaments of approximately 80 Å in diameter. Classical TCP form rope-like bundles, in which filaments are aligned along their length and associate via extended lateral interactions (Figure 4.3). In contrast, El Tor TCP interact in an orthogonal manner, with individual filaments crossing over each other to form a “crossroads” pattern. This pattern is detected for El Tor strain C6706, and more dramatically for partially purified El Tor TCP from the classical biotype, RT4340, which has been engineered to express El Tor TcpA (Figure 4.3). The crossroads pattern of interactions seen with the El Tor TCP has not been reported for other pili.

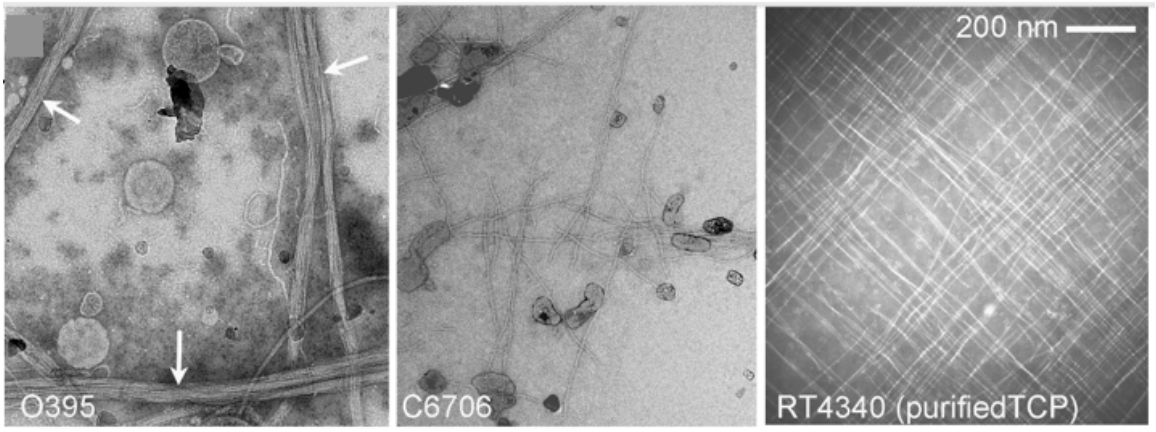

Figure 4.3 **Morphology and bundling characteristics of *V. cholerae* TCP by TEM.** Classical O395 and El Tor C6706 micrographs are from whole cell culture whereas the RT4340 micrograph represents partially purified TCP. Classical TCP (O395) form rope like bundles, whereas El Tor TCP (C6706, RT4340) form a crossroads pattern. Scale bar for all panels, 200 nm.

To understand the dramatic difference in the pilus interaction patterns, I compared the pilin structures from the two biotypes. The non-conserved residues between classical and El Tor TcpA are localized to two patches on the surface of the globular domain (Figure 4.4).

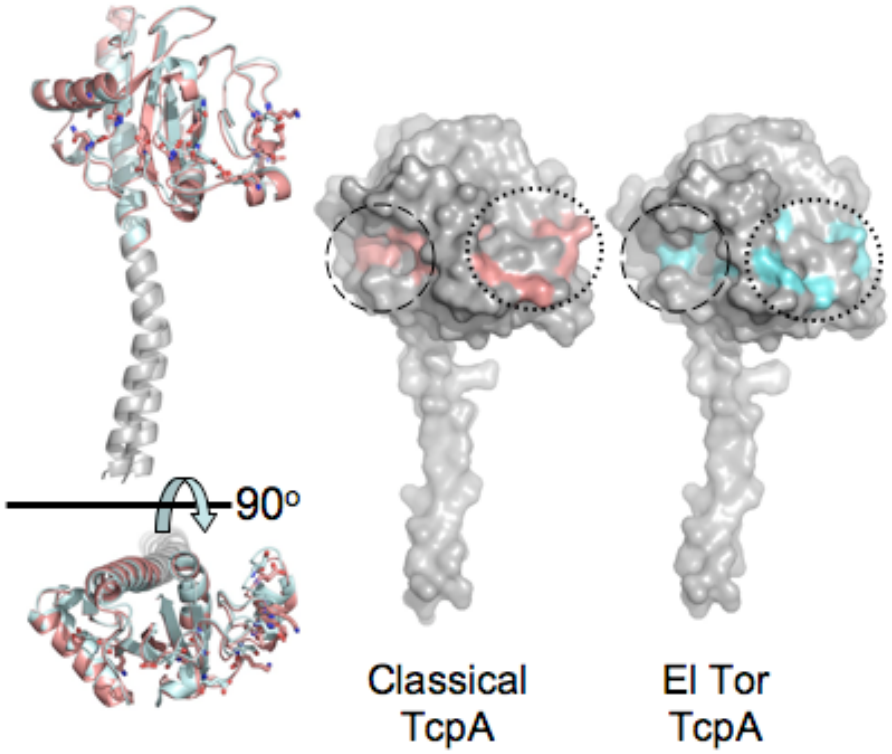

Figure 4.4 Non-conserved residues are localized to the surface of the globular domain (circled). In ribbon representation of classical (salmon) and El Tor (cyan) TcpA, non-conserved residues are represented as sticks. Since the TcpA crystal structures lack the N-terminal α-helices (α1N), these were modelled on the full length PAK pilin (Craig *et al*., 2003).

Also, comparison of the electrostatic surface of classical and El Tor TcpA revealed a patch in the D-region (Figure 1.4) that differ substantially between the two proteins, having an overall positive charge in classical TcpA and a negative

charge in El Tor TcpA (Figure 4.5). Most of the non-conserved amino acids lie on this patch and represent changes from a non-charged residue to charged one, or *vice versa*: A138E, A156D, E158A, K172A, D175N and K187T (corresponding residues in classical and El Tor TcpA, respectively). Several of these changes are from alanine to a bulky charged residue, or *vice versa*, which alters the stereochemistry of the D-region surface. The D-region of classical TcpA is exposed to solvent in the TCP filament, with residues ~145-183 being the most exposed residues (Li *et al*., 2008), as determined by hydrogen/deuterium exchange mass spectrometry. Thus, amino acid changes in the D-region of TcpA may have a profound effect on the chemistry and structural landscape of the TCP surface, given that they are present in each of the thousands of subunits that make up the filament. We hypothesized that residues in the D-region patch are directly involved in pilus:pilus interactions and thus responsible for the difference in interaction patterns observed for classical and El Tor TCP filaments.

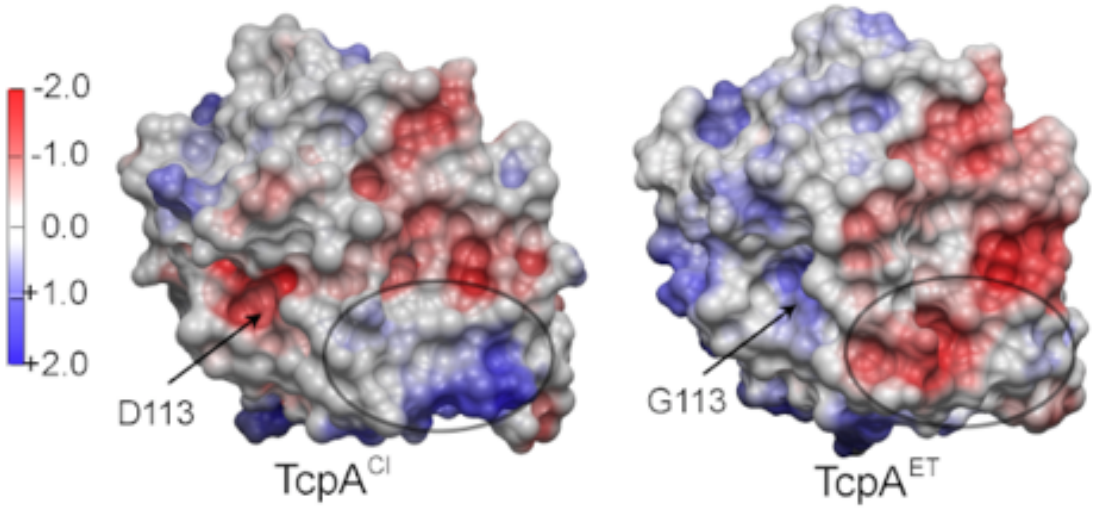

Figure 4.5 Comparison of the electrostatic surface of TcpA from classical and El Tor biotype, shown in the same orientation as Figure 4.4. The electrostatic surface differs in the D-region patch (circled). There are six non-conserved amino acid differences between the two proteins, each resulting in a change (gain or loss) of charge. A second difference is in the location of an aspartate to glycine change at residue 113.

To further understand the effects of this amino acid differences in pilus:pilus interaction, I compared the computational TCP model between the two biotypes (Figure 1.5). The El Tor TCP model was generated by fitting the El Tor TcpA structure into the classical TCP model generated previously based on solvent accessibility, TCP symmetry parameters and crystal packing of the TcpA classical subunit (Li *et al*., 2008; Craig *et al*., 2003). In the TCP models, the N-terminal α-helices form a hydrophobic core anchoring the globular domains, which are loosely packed on the filament surface creating pronounced gaps or cavities between the subunits (Figure 1.5). The $\alpha\beta$-loop edge of the globular domain is turned inward toward the core of the filament and is in contact with the N-terminal α-helix of a neighbouring subunit (Figure 3.2). The D-region edge of

the globular domain is turned outward and forms a slight bulge or protrusion on the filament surface, making minimal contact with the neighbouring subunits (Figure 3.2, Figure 4.6). The filament models clearly placed the non-conserved residues on the exposed face of the pilin subunits (Figure 4.6). Exposed residues lining the cavities between the subunits are for the most part conserved, with the exception of residue 113, which is an aspartate in classical TcpA and a glycine in El Tor TcpA (Figure 4.6).

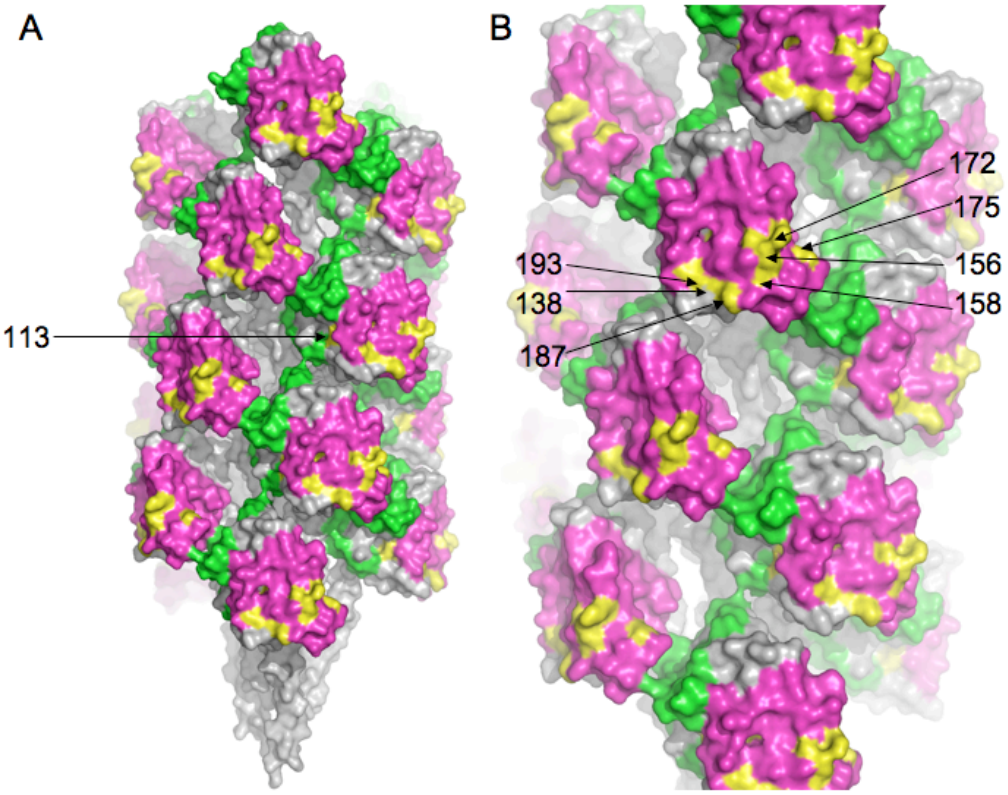

Figure 4.6 **Model of the classical TCP filament.** Space-filling representation of classical TCP shows non-conserved amino acids (yellow) are (A) in the cavity of the filament (113) and (B) on the protruding D-region. D-region residues 138, 156, 158, 172, 175 and 187 were selected for classical-to-El Tor changes, as was cavity residue 113.

From the comparison of TcpA and TCP filament surfaces, we hypothesized that the different pilus:pilus interaction phenotypes result from the non-conserved amino acid differences between classical and El Tor biotypes, that lie almost exclusively on the protruding D-region. To test this hypothesis, these six prominent surface exposed residues were replaced in classical TcpA to their corresponding residues in El Tor TcpA, both individually and in combination.

4.2 Results

To assess the role of the exposed, non-conserved residues in pilus:pilus interaction, I focused on the six residues in the protruding part of the D-region that either gain or loose a charge between classical and El Tor TcpA: A138E, A156D, E158A, K172A, D175N and K187T (Figure 4.6). Each of these six D-region residues in classical TcpA was changed to its corresponding residue in El Tor TcpA, both individually and as composite mutations (Table 2). All mutations were made by site-directed mutagenesis as described in Chapters 2 and 3. *V. cholerae* strain ML7 and ML10 were used as positive and negative controls as described in Chapter 3.

Table 2 Mutant phenotypes

Bacteria	Description	Pilin	Pili	AA*	Pilus:pilus interactions (EM)
V. cholerae O395	Wild type, classical (O1 classical strain)	+	+	+++	ropes
V. cholerae ML7	RT4524, Classical TcpA	+	+	+++	ropes
V. cholerae C6706	Wild type, El Tor	+	+	-	crossroads
V. cholerae RT4524	Classical tcpA::*lacZ*	-	-	-	-
V. cholerae RT4340	Wild type El Tor TCP on *V. cholerae* O395	+	+	+++	crossroads
V. cholerae ML10	C120A	-	-	-	-
	D-region Classical to El Tor mutations				
V. cholerae LC1	A138E	+	+	+++	ropes
V. cholerae LC6	K187T	+	+	+++	ropes
V. cholerae ML12	D175N	+	+	-/+	ropes
V. cholerae ML15	**A156D**	+	+	+++	crossroads
V. cholerae ML17	E158A	+	+	+++	ropes
V. cholerae ML18	K172A	+	+	+++	ropes
V. cholerae LC7	**A156D**/E158A	+	+	+++	ropes/crossroads
V. cholerae ML14	K172A/D175N	+	+	+++	ropes
V. cholerae LC9	A138E/**A156D**/E158A	+	+	+++	ropes/crossroads
V. cholerae LC10	A138E/**A156D**/E158A/K172A	+	+	+	ropes/crossroads
V. cholerae LC11	A138E/**A156D**/E158A/K187T	+	+	-/+	ropes/crossroads
V. cholerae LC12	**A156D**/E158A/K172A/D175N	+	+	-/+	ropes/crossroads
V. cholerae ML16	A138E/**A156D**/E158A/K172A/K187T	+	+	-	crossroads
V. cholerae LC13	A138E/**A156D**/E158A/K172A/D175N	+	+	-/+	ropes/crossroads
V. cholerae LC15	**A156D**/E158A/K172A/D175N/K187T	+	+	+++	ropes/crossroads
V. cholerae LC16	A138E/**A156D**/E158A/K172A/D175N/K187T	+	+	-	crossroads
V. cholerae ML25	LC16 with D156A	+	+	+++	ropes
	Cavity mutants				
V. cholerae ML9	D113A	+	+	-	crossroads
V. cholerae ML28	D113G (Classical to El Tor)	+	+	-	ropes
*AA=autoagglutination					

All mutants were examined for pilin production, pilus assembly, pilus morphology, bundling interactions, autoagglutination and their ability to interact with CTXϕ. For assaying autoagglutination, RT4340 strain, which is a classical strain O395, expressing El Tor TcpA, was used as a control since El Tor strains produce significantly reduced level of TCP compared to classical strains in laboratory conditions (DiRita *et al*., 1996).

All the mutations produced wild type levels of TcpA as well as assembled pili, as detected by immunoblot analysis (Table 2, Figure 4.7). All of the single mutants autoagglutinated to the wild type levels with the exception of D175N (ML12), which produced reduced levels of autoagglutination. Some but not all of

the composite mutations showed reduced levels of autoagglutination. In general, the more mutations present, the lower the autoagglutination levels, although strains LC15 and ML25, which both have 5 classical-to-El Tor mutations showed wild type autoagglutination levels. It is important to note that the appearance of pilus:pilus interactions by TEM did not always correlate with autoagglutination. All of the mutants appeared to interact by TEM, either in rope-like bundles, a crossroads pattern or a combination of the two, yet several of the mutants (strain ML12, LC10, LC11, LC12, LC13, ML16, LC16, ML9 and ML28) autoagglutinated poorly or not at all. This suggests that autoagglutination requires tight pilus:pilus interactions, which cannot be discriminated from weak interactions by TEM.

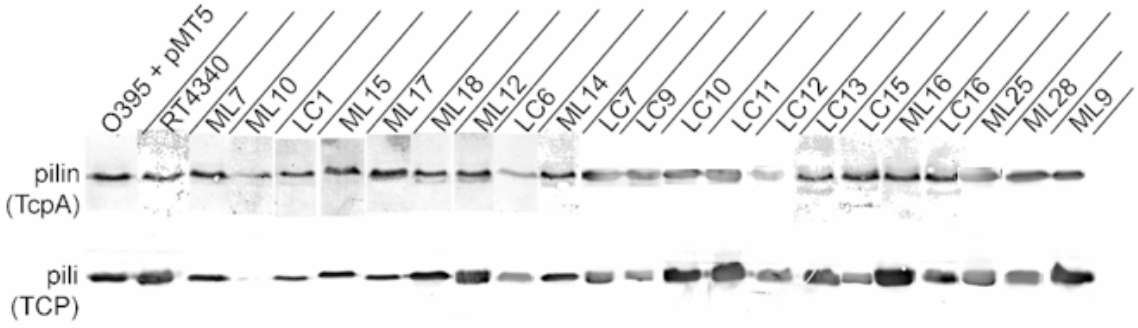

Figure 4.7 Analysis of classical-to-El Tor mutants for pilin and pilus expression. Expression of TcpA (upper panel) and TCP (lower panel) in mutant strains compared to the wild type controls. Pilin bands were detected in whole cell cultures and pilus bands were detected from sheared cell supernatants. All mutants, with the exception of strain ML10, produced TcpA and TCP at approximately wild type levels, indicating that the mutations do not affect pilin fold or pilus assembly. A proteolytic degradation product was occasionally observed for both the wild type strains and mutants.

All mutants were assessed by TEM to study morphologies of pili and their interaction patterns (Table 2, Figure 4.8). The TCP filament morphologies of the mutants were similar to the wild type, being long and relatively straight. For all of

the single mutants, TCP interacted in rope-like bundles, characteristic of the classical strain, with the exception of A156D (ML15), which displayed the El Tor crossroads pattern of interaction. Furthermore, every composite mutant containing the A156D mutation also showed the El Tor interaction phenotype, although rope-like bundles were also present for some of these strains (Table 2). These results implicate residue 156 as a key determinant in pilus:pilus interactions. To test the involvement of residue 156 in pilus:pilus interactions, I changed D156 back to alanine in the six-residue composite TcpA mutant strain, LC16 (A138E/**A156D**/E158A/K172A/D175N/K187T), resulting in strain ML25 (A138E/E158A/K172A/D175N/K187T). LC16 had mostly crossroads but ML25, with the single amino acid change, resulted in a shift in the TCP interactions from the crossroads pattern, characteristic of El Tor TCP, to the rope-like bundles seen for classical TCP (Figure 4.8). Furthermore, autoagglutination levels were restored to wild type levels in this strain suggesting a strengthening of the pilus:pilus interactions. This result further confirmed residue 156 as a key factor in pilus:pilus interaction.

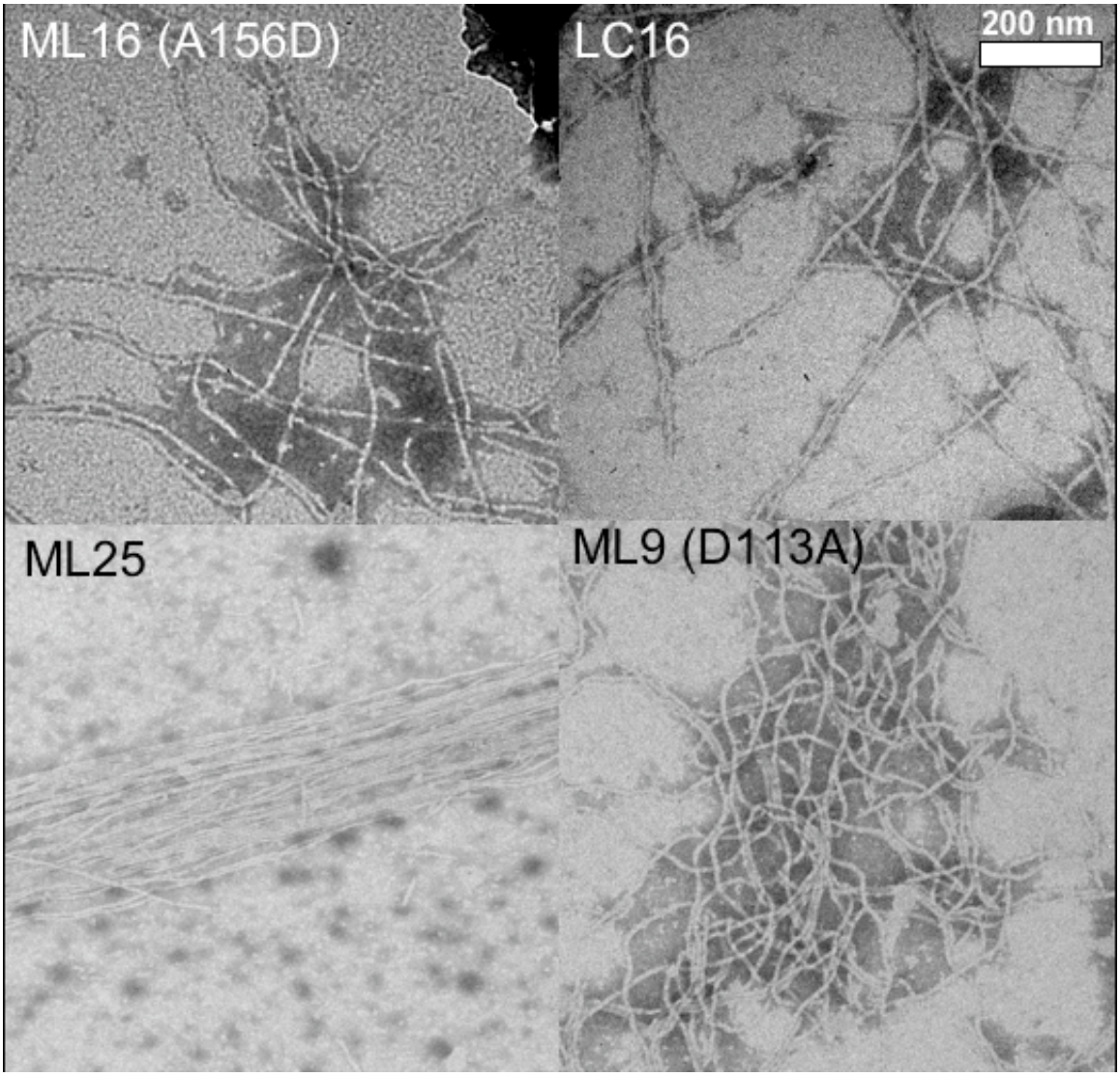

Figure 4.8 **TEM images of TCP from mutants.** The single A156D mutant ML15, the complete classical to-El Tor surface patch mutant LC16 (A138E/A156D/E158A/K172A/D175N/K187T), and the single D113A mutant ML9, display a crossroads pattern. The D156A reversion of LC16 strain, ML25, is mainly rope like bundles. Scale bar for all panels, 200 nm.

Residue156 is among the most prominent residues on the surface of the TCP filament model from both of the biotypes, lying on the partially protruding D-region (Figure 4.6). We hypothesized that residue 156 and other residues on the D-region protrusions of one filament interact with the depressions or cavities

formed between the subunits in adjacent filaments, causing the pili to aggregate. While there are several residues on the protruding D-region that differ between classical and El Tor biotypes, the residues that line the cavity are conserved, with the exception of residues 92 and 113, which are ~10 Å apart. These residues have bulky polar and charged side chains asparagine and aspartate, respectively, in classical TcpA, and small-uncharged side chains alanine and glycine, respectively, in El Tor TcpA. I changed D113 to glycine in classical TcpA (ML28), which had no apparent effect on pilus expression or pilus:pilus interaction pattern. However, a D113A mutation (ML9) resulted in a poorly-autoagglutinating strain with the crossroads TCP interaction pattern (Figure 4.8). The results for D113A suggest that this cavity is also involved in pilus:pilus interactions.

Each mutant was also tested for its ability to interact with CTXϕ. These results will be discussed in Chapter 5.

4.3 Discussion

Type IV pilus-mediated bacterial aggregation is common to many bacterial pathogens and an essential step in colonization and pathogenesis. However, the molecular mechanism behind this pilus:pilus interaction is not well understood. To understand the molecular basis for pilus-mediated microcolony formation, I explored the differences between TCP of *V. cholerae* classical and El Tor biotypes. I observed that the two biotypes have different pilus:pilus interaction patterns; classical TCP form rope-like bundles whereas El Tor TCP form crossroads patterns. These patterns of interaction have also been observed in

three-dimensions by field emission scanning EM (Taylor and Krebs, unpublished data), suggesting that it is not an artefact of our negative stain imaging methods. Interestingly, these arrangements can be altered by single amino acid substitutions indicating that pili associate with each other in a highly specific manner. Also the fact that both *V. cholerae* biotypes are effective colonizers capable of causing cholera disease in humans, indicates that both the lateral and the orthogonal interactions are effective in holding cells together in microcolonies.

From the mutational studies, key determinants in pilus:pilus interactions lie on the bulge (residue 156) and in the cavity (residue 113) of the TCP filament. The A156D (ML15) mutation is remarkable in that this single amino acid change can shift the pilus:pilus interactions from lateral to orthogonal ones. ML15 also autoagglutinates well. The ML15 phenotype is indistinguishable from that of RT4340, the classical *V. cholerae* strain that over-expresses El Tor TcpA. Conversely, strain ML25, which has an alanine at position 156, as in classical TcpA, but has El Tor residues at each of the other five D-region patch positions, autoagglutinates well via rope-like pilus:pilus interactions. The ML25 phenotype is indistinguishable from that of O395, the classical *V. cholerae* wild type strain. The D113A mutation (ML9) within the cavity resulted in complete conversion of the pilus:pilus interactions from rope-like bundles to the crossroads pattern, suggesting that this residue is a determinant in pilus:pilus interactions. However, it is not clear why the D113G mutation (ML28) did not result in a noticeable effect on the pilus:pilus interaction pattern. Perhaps, the mutation to glycine allowed

more flexibility in the polypeptide backbone around residue 113, allowing it to accommodate the D-region bulge more readily than would an alanine at this position. To explain how single mutations such as A156D and D113A dramatically shift the orientation of pili in microcolonies, I propose that for classical TCP, the D-region bulge has a shape and chemistry that allows it to intercalate between the subunits of adjacent TCP when the filaments associate laterally and twist around each other, whereas in El Tor TCP, this complementarity is achieved only when the pili lie orthogonally to each other (Figure 4.9). Introducing an aspartate at residue 156 of classical TcpA, D156, alters the shape and chemistry of the D-region bulge. This change disrupts the complementarity between the bulges and cavities when the filaments are oriented laterally, but when one filament orients itself at 90° to the other, the bulges can now fit into the cavities. Multiple classical to El Tor mutations in the D-region are apparently tolerated, as both crossroads and rope like bundling interactions are observed (Table 2), but these interactions are typically weaker, as demonstrated by the poor autoagglutination phenotypes of these mutants and presumably require further classical to El Tor mutations in the cavities to optimize these interactions.

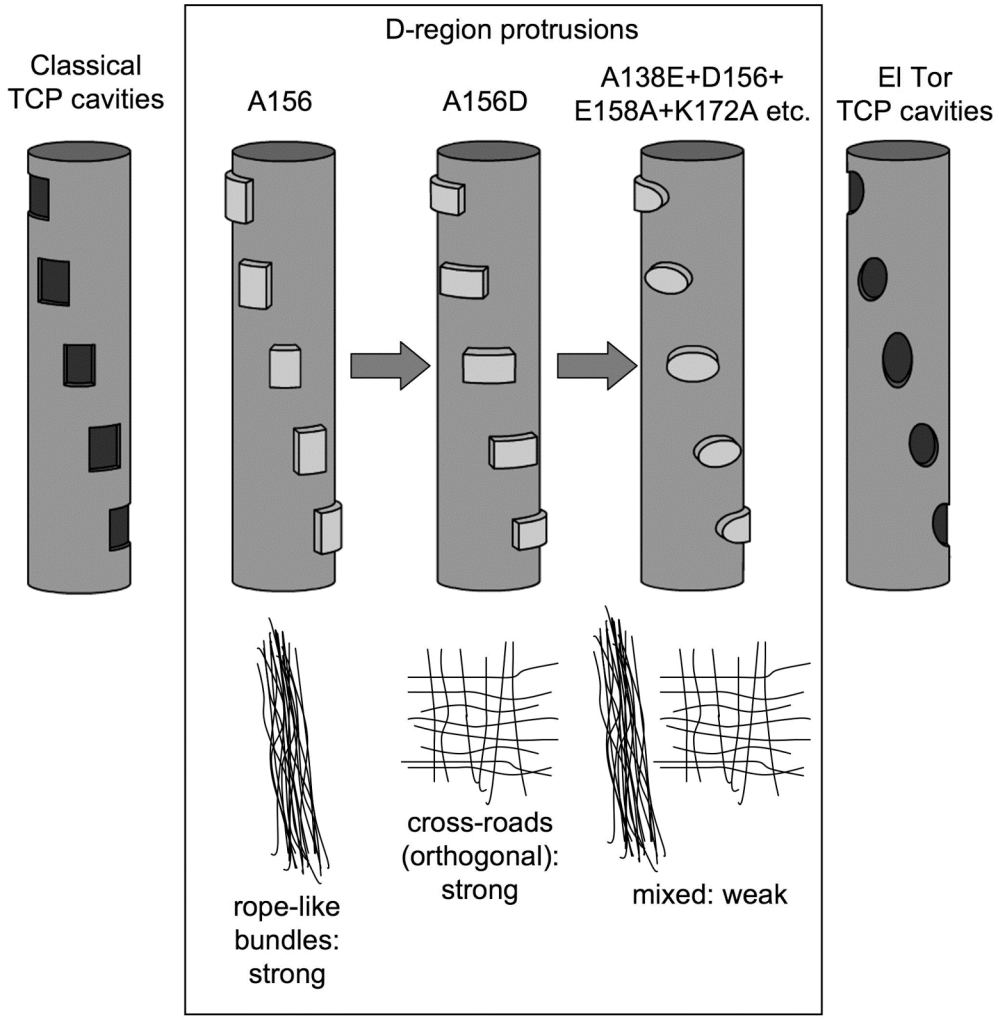

Figure 4.9 **Intercalation model for TCP:TCP interactions.** Substantial amino acid differences on the D-region protrusions and minor differences in the cavities between the globular domains result in surfaces that differ between classical and El Tor TCP. The D-region protrusions of classical TCP are complementary in shape and chemistry to their cavities when the filaments associate laterally, in rope-like bundles. Such interactions are strong enough to autoagglutinate cells. The A156D mutation in classical TcpA changes the D-region protrusion such that it now fits into the cavities only when the filaments associate orthogonally, in a crossroads pattern, this interaction is also sufficiently strong to autoagglutinate cells. Multiple classical-to El Tor mutations alter the D-region protrusion such it is no longer perfectly complementary to the cavities, regardless of the orientation of the pili. Both rope-like bundles and crossroads patterns are observed but these interactions are not strong enough to autoagglutinate cells. These multiple mutations in the protruding D-region would require complementary mutations, presumably in the cavities, to optimize these interactions and allow for autoagglutination.

CHAPTER 5: PILUS:CTXϕ INTERACTIONS

5.1 Introduction

The biomedical importance of understanding the life cycle of bacteriophages has increased with the discovery that many of these bacteriophages carry the virulence genes that confer pathogenesis of an organism. A better understanding of the infection mechanism of filamentous bacteriophages, especially the crucial, initial recognition step of the target pilus by the phage virions, has important implications for the understanding of such bacterially transmitted diseases.

CTXϕ is a *V. cholerae* specific filamentous bacteriophage that carries genes encoding cholera toxin, a potent enterotoxin that causes the severe diarrhea, the hallmark of cholera. Thus, acquisition of CTXϕ was the key event in the emergence of *V. cholerae* as a human pathogen. *V. cholerae* strains lacking TCP are not susceptible to CTXϕ infection indicating TCP as a receptor for CTXϕ (Waldor *et al*., 1996; Kirn *et al*., 2000; Li *et al*., 2008). However, biochemical or EM evidence of CTXϕ virions binding to TCP is lacking, and the mechanism by which CTXϕ binds to TCP is not understood. Waldor *et al*. (2003) showed that pIII of CTXϕ is required for the entry and release of CTXϕ into *V. cholerae* using engineered fd-pIII CTXϕ (Waldor *et al*., 2003). They showed that by introducing segments of pIII from CTXϕ onto *E. coli* fd phage, this engineered fd-pIII CTXϕ was able to infect *V. cholerae*. However, they were unable to demonstrate a

direct interaction between fd-pIII CTXϕ and TCP. Owing to the lack of structural information on CTXϕ, little is known about the molecular basis of the interaction between the CTXϕ pIII and TCP. Also, it cannot be ruled out that the CTXϕ major coat protein, Cep, is involved in initial binding of CTXϕ and TCP.

The immuno-gold TEM analysis *in vitro* offers a direct measure of the TCP:CTXϕ interactions, by detecting the initial binding of CTXϕ to TCP. On the other hand, the infectivity assay, CTXϕ transduction assay *in vivo,* depends on the interaction between the phage and the pilus, followed by a succession of other events that leads eventually to phage production and secretion. Therefore, I used both methods to study the molecular mechanisms involved in TCP:CTXϕ interactions. For the transduction assay, mutant strains described in Chapter 4 were used to pinpoint the residues involved in TCP:CTXϕ interaction. On the other hand, since the same CTXϕ virion can infect both classical and El Tor *V. cholerae*, it may be that the residues in TcpA involved in this interactions are conserved between the two biotypes. To test this hypothesis some of the surface-exposed, conserved residues between the two biotypes were also changed.

5.2 Results

5.2.1 Infectivity assay to assess ability of TcpA mutants to bind CTXϕ

In an attempt to elucidate regions within TcpA responsible for interactions with the CTXϕ, the transduction assay was performed on each of the classical-to-El Tor mutants described in Chapter 4 (Table 2). Since CTXϕ is not a plaque-

forming phage, virion production was detected by the ability of supernatants from a strain containing an El Tor CTXϕ that carries the kanamycin resistance marker (CTX-Kanϕ) to transform the recipient *V. cholerae* strains, which are streptomycin resistant, Sm^R, into Sm^RKan^R. Upon infection, El Tor CTXϕ replicates as a plasmid in classical *V. cholerae* strains. Transduction frequency (page 27) was determined as the fraction of transconjugants among recipients, as measured by the number of Kan^RSm^R colony forming units (cfu) divided by Sm^R cfus (Waldor *et al*., 1997). Transduction efficiency was calculated as a fraction of transduction frequency of a mutant strain relative to the transduction frequency of the wild type, O395 strain.

Three of the classical-to-El Tor D-region mutants, ML9 (D113A), ML2 (V161A), and ML12 (D175N) showed a substantial decrease in their ability to transduce CTXϕ. None of the other single classical-to-El Tor D-region mutations produced a dramatic effect on phage transduction (Table 3). LC1 (A138E) and ML18 (K172A) showed higher CTXϕ transduction frequencies than the wild type. Some of the composite mutants were substantially reduced in phage transduction. Strains LC12, LC13, and LC16 showed the highest decrease in transduction frequency among the composite mutation group. Other composite mutants were moderately affected whereas LC9, with 3 mutations, showed a higher CTXϕ transduction frequency than the wild type, O395.

To test the hypothesis that CTXϕ interaction involves conserved residues on TcpA between the two biotypes, select conserved residues on the surface of TcpA were changed to alanine, and to aspartate if the original residue was

alanine (Table 3). Lys85 was changed to alanine and also to the negatively-charged glutamate, to assess the charge requirement at this site. None of the conserved residue mutations (T159A, A102D, K85E, K85A) showed dramatic effects on CTXϕ binding.

Table 3 CTXϕ transduction efficiency

Bacteria	Description	AA[1]	Transduction efficiency[2]
V. cholerae O395	Wild type, classical (O1 classical strain)	+++	1
V. cholerae ML 7	RT4524, Classical TcpA	+++	1.04
V. cholerae C6706	Wild type, El Tor	-	0.23
V. cholerae RT4524	Classical tcpA::*lacZ*	-	0
V. cholerae RT4340	Wild type El Tor TCP on *V. cholerae* O395	+++	0.35±0.01
V. cholerae ML10	C120A	-	0
	Conserved surface exposed mutations		
V. cholerae ML 8	T159A	-/+	0.68±0.17
V. cholerae ML 11	A102D	++	0.76±0.17
V. cholerae ML 29	K85E (pocket)	+++	0.31±0.12
V. cholerae ML 30	K85A (pocket)	+++	0.40±0.05
	Pilus:pilus interaction (Chapter 4)		
	D-region Classical to El Tor mutations		
V. cholerae LC1	A138E	+++	1.45±0.28
V. cholerae LC6	K187T	+++	0.53±0.38
V. cholerae ML12	D175N	-/+	0.02±0.01
V. cholerae ML15	A156D	+++	0.55±0.05
V. cholerae ML17	E158A	+++	0.70±0.09
V. cholerae ML18	K172A	+++	1.54±0.28
V. cholerae LC7	A156D/E158A	+++	0.20±0.06
V. cholerae ML14	K172A/D175N	+++	0.39±0.19
V. cholerae LC9	A138E/A156D/E158A	+++	1.49±1.24
V. cholerae LC10	A138E/A156D/E158A/K172A	+	0.32±0.19
V. cholerae LC11	A138E/A156D/E158A/K187T	-/+	0.39±0.35
V. cholerae LC12	A156D/E158A/K172A/D175N	-/+	0.06±0.02
V. cholerae ML16	A138E/A156D/E158A/K172A/K187T	-	0.15±0.04
V. cholerae LC13	A138E/A156D/E158A/K172A/D175N	-/+	0.02±0.01
V. cholerae LC15	A156D/E158A/K172A/D175N/K187T	+++	0.10±0.06
V. cholerae LC16	A138E/A156D/E158A/K172A/D175N/K187T	-	0.03±0.03
V. cholerae ML25	LC16 with D156A	+++	0.22±0.00
V. cholerae ML 2	V161A	-/+	0.05±0.01
	Cavity mutants		
V. cholerae ML9	D113A	-	0.004±0.002
V. cholerae ML28	D113G (Classical to El Tor)	-	0.25±0.04

[1]Autoaggluitnation. [2]Transduction efficiency is presented as an average of two or three separate CTXϕ transduction assays and standard errors are represented based on standard deviation to the mean. Transduction frequency is calculated based on the number of CTX-Kanϕ transductants per input cfu and is presented as efficiency relative to the wild type.

From the infectivity assay, it appears that the mutations that affect CTXϕ infection are in non-conserved residues between the two biotypes (Figure 5.1).

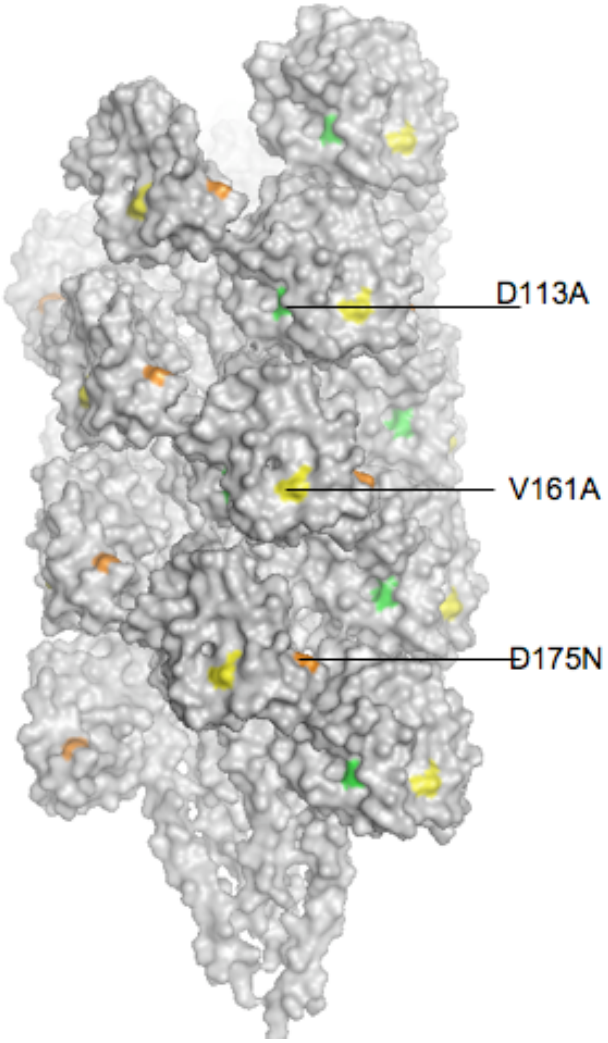

Figure 5.1 **TCP:CTXϕ interaction.** Space-filling representation of TCP model from *V. cholerae* classical strain. The three single mutations that showed dramatic decrease in CTXϕ infection are indicated. They are distributed across the TcpA surface.

5.2.2 Immuno-gold labelling to image TCP:CTXϕ interactions

From the infectivity assay, it was difficult to speculate on the mechanism of CTXϕ binding to TCP. To better understand the molecular basis for TCP:CTXϕ interaction, I directly visualized the TCP:CTXϕ interaction by TEM. If CTXϕ bind to TCP via their tips, it would implicate pIII or other minor coat proteins as the major phage adhesin. TCP and CTXϕ look identical by TEM, both being long filaments that are ~8 nm in diameter. To distinguish TCP from CTXϕ, I used immuno-gold labelling. Filaments were incubated with their respective antibodies or were biotinylated followed by incubation with a secondary antibody conjugated with different sized gold particles (Figure 2.4).

CTXϕ was purified by PEG/NaCl precipitation of filtered supernatant containing CTXϕ after overnight growth of *V. cholerae* RT4236. RT4236 lacks flagella, which interfere with imaging the phage. The culture was grown under non-pilus expressing conditions, which eliminates the possibility of contamination by TCP.

To image TCP:CTXϕ interactions, TCP were purified from whole cell cultures, as described in Chapter 2. TCP used in this study have a mutation in the TcpA subunit, H181A, which causes them to be shed into the culture supernatant for large-scale purification. TCP^{H181A} filaments from whole cell culture resemble wild type TCP by negative stain TEM and share the same quaternary structure (Li *et al*., 2008). Importantly, H181A mutant showed transduction efficiency similar to the wild type (Kirn *et al*., 2000), indicating that TCP^{H181A} maintains its ability to interact with CTXϕ.

To label TCP and CTXϕ with different sized gold particles for each filament type, the primary antibodies against each filament had to be from different host animals, otherwise the secondary antibodies would bind to both primary antibody types. Antibody against CTXϕ was raised by immunizing rabbits with the N-terminal peptide of the major coat protein, Cep, of CTXϕ (Pacific Immunology). Rabbit anti-Cep antibodies successfully labelled CTXϕ (Figure 5.2A). To label TCP with gold conjugated antibodies, TCP was biotinylated. Biotinylated proteins can be labelled with streptavidin conjugated gold particles. However, TEM studies showed that streptavidin does not label biotinylated TCP. It was found that goat anti-biotin is a more sensitive detector of biotin compared to streptavidin when conjugated to gold particles (RDI, 1997). Goat anti-biotin successfully labelled biotinylated TCP (Figure 5.2B).

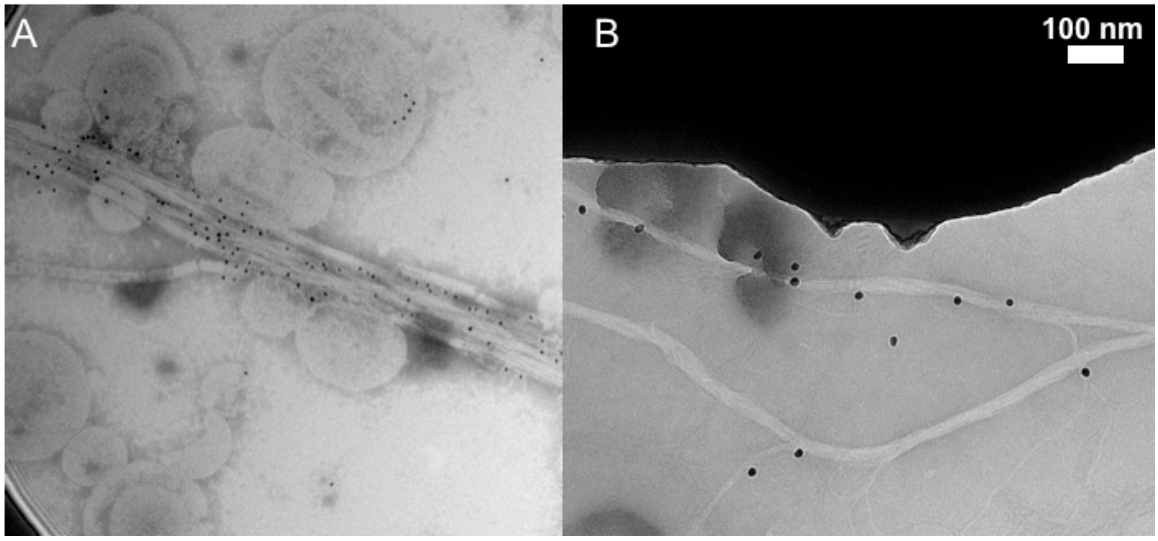

Figure 5.2 Immuno-gold labelling. TEM images of (A) CTXϕ with 10-nm gold particles and (B) biotinylated TCP^{181A} with 20-nm gold particles**.** Scale bar for all panels, 100 nm.

As a negative control, biotinylated TCP were incubated with rabbit anti-Cep antibody followed by incubation with goat anti-rabbit antibody conjugated with 10-nm gold particles (Figure 5.3A). There was no non-specific binding of anti-Cep antibody to the biotinylated TCP. CTXϕ was incubated with anti-biotin antibody conjugated with 20-nm gold particles. While there was considerable binding to the carbon matrix, none of the CTXϕ filaments were associated with gold particles (Figure 5.3B).

After optimizing conditions for the single labelling of each filament, TCP and CTXϕ were incubated together and then this mixture was applied onto a nickel grid. The grid was immuno-gold labelled in two steps. First, the grid was incubated with goat anti-biotin antibody conjugated with 20-nm gold to label biotinylated TCP. Second, the grid was incubated with rabbit anti-Cep antibody followed by goat anti-rabbit antibody conjugated with 10-nm gold to label CTXϕ. Few filaments were observed for these grids, but those that were observed had both the 10 nm and the 20 nm gold particles associated, with only low levels of background binding (Figure 2.4, Figure 5.3C, D). In these images, the filaments occur in small rope-like bundles, suggesting that CTXϕ and TCP interact all along the length of the filament, similar to TCP:TCP interactions. While these results are very preliminary and require further study, they support the idea that the major coat protein, Cep, is involved in CTXϕ-TCP interactions.

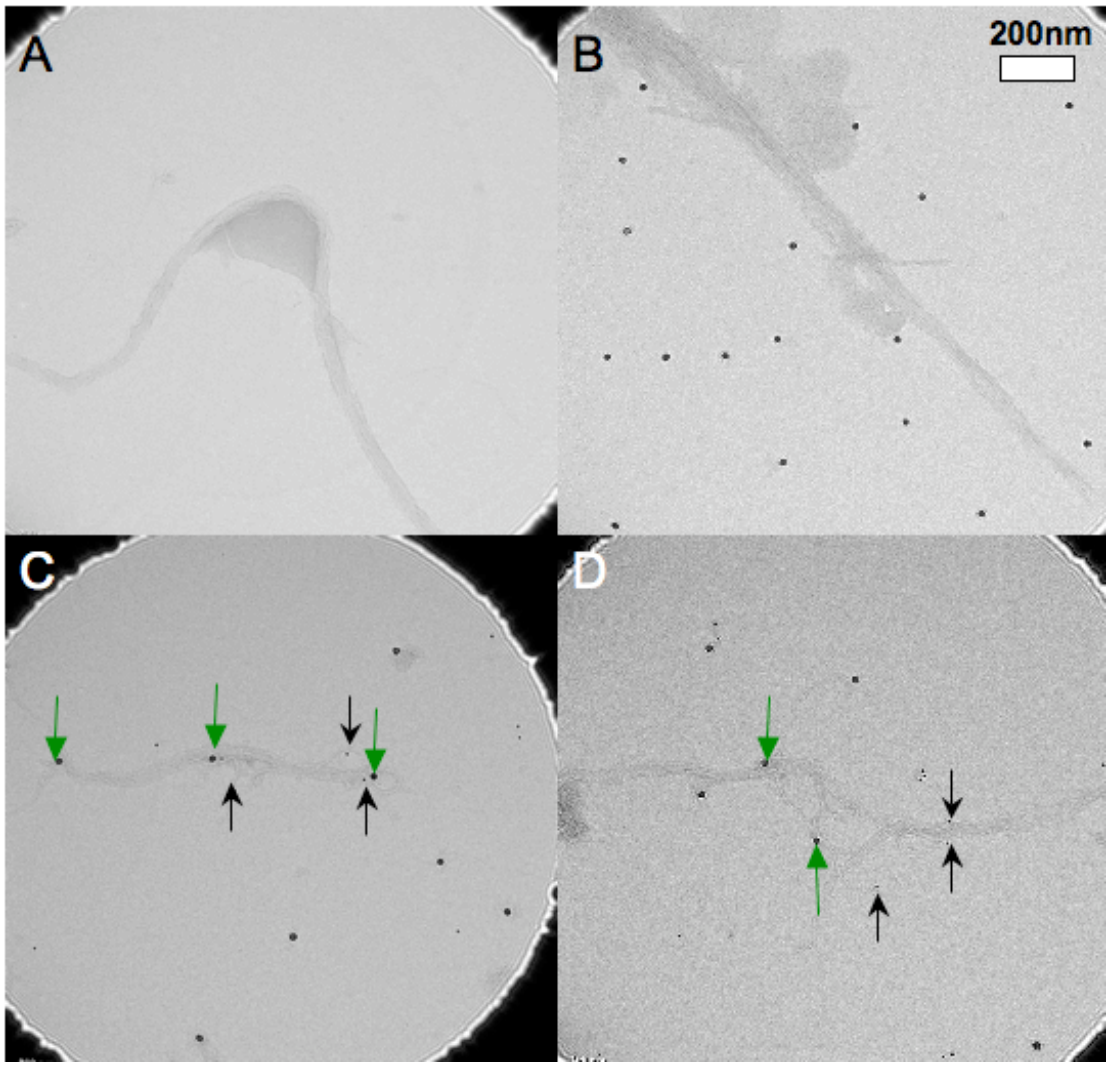

Figure 5.3 Immuno-gold labelling of TCP interacting with CTXϕ. (A) Negative control where TCP is labelled with anti-CTXϕ antibody. (B) Negative control where CTXϕ is labelled with anti-biotin antibody. No specific binding is observed in either (A) nor (B). (C, D) Mixture of TCP and CTXϕ was labelled as described in Figure 2.4. Small gold particles (black arrow) label CTXϕ and larger gold particles (green arrow) label TCP. Scale bar for all panels, 200 nm.

5.3 Discussion

The nature of the interactions between CTXϕ and TCP was investigated using site-directed mutagenesis of TcpA and CTXϕ transduction assays and TEM analyses. In this study, I have identified a subset of amino acid residues on TcpA

as being involved in the binding of CTXϕ to TCP. Furthermore, I provide the first microscopic evidence of TCP:CTXϕ interactions.

From the CTXϕ transduction assays, three single mutations showed a substantial decrease in CTXϕ uptake (Figure 5.1). Since the infection of CTXϕ depends on the amount of TCP, surface expressed TCP was quantified by immunoblotting sheared pili from whole cell cultures. All the mutants showed comparable levels of TCP, indicating that the decrease in CTXϕ transduction efficiency is not due to decreased amount of TCP but rather, decreased binding efficiency of CTXϕ to TCP. No gross differences in TCP morphology were noted by TEM: the mutant TCP were similar in appearance to the wild type TCP, all being long and relatively straight, with the exception of D113A, which appeared slightly wavy (Figure 4.8). It is surprising that some of the single classical-to-El Tor changes, such as D175N, V161A and D113A, showed a substantial decrease in CTXϕ binding. Also, a few composite classical-to-El Tor mutations (LC12, LC13, and LC16) resulted in a dramatic decrease in CTXϕ infection. D175N and other single residue changes, D113A and V161A, that showed a dramatic decrease in CTXϕ infection, are located far apart from each other (Figure 5.1). This suggests that CTXϕ binding occurs over a large surface of TcpA. This is supported by my TEM images, which showed extensive lengthwise interactions between TCP and CTXϕ. Interestingly, all the mutations that showed a decrease in CTXϕ infection also showed a decrease in autoagglutination. This

might suggest that these mutants have changes in the overall chemistry of pilus morphology, which likely caused the decrease in CTXϕ transduction.

Immuno-gold TEM analyses showed that CTXϕ binds to TCP all along its length (Figure 5.3 C, D). These data suggest that the CTXϕ major coat protein, Cep, is involved in TCP:CTXϕ interaction. However, Waldor *et al*. (2003) showed that segment of minor coat protein, pIII, is enough to confer infectivity of engineered fd-pIII CTXϕ (Waldor *et al*., 2003). Perhaps, the initial binding of CTXϕ to TCP is achieved by its major coat protein, Cep, and then pIII binding to TCP follows.

Here, I used site-directed mutagenesis on surface residues of TcpA protein, and evaluated the effects on the binding of CTXϕ by means of infectivity *in vivo* and immuno-gold labelling *in vitro*. This work suggests that (i) CTXϕ binds to a large surface on TcpA rather than to a discreet patch; and (ii) CTXϕ interacts with TCP along its entire length, rather than just via its minor coat protein, pIII, which is predicted to be tip-associated. The work presented here provides a starting point and a methodology for investigating TCP:CTXϕ interactions.

CHAPTER 6: CONCLUSION AND FUTURE PROSPECTS

The nature of TCP interactions have been investigated by defining discrete regions of the pilin subunit that are directly involved in pilus assembly, and pilus-mediated bundling, microcolony formation and CTXϕ interactions. The structural analyses of the pilin subunits and the computational TCP models from both classical and El Tor *V. cholerae* biotypes provided the framework for designing select mutations that affect TCP assembly and interactions. The rationale behind the efforts to examine the key virulence factor of *V. cholerae* TCP is to gain new knowledge and eventually devise means to control cholera epidemics.

Identification of residues that have a dramatic effect on pilus production, provided clues in pilin:pilin interactions during pilus assembly. This study shows that disruption of ionic or hydrophobic interactions between the small interface, αβ-loop:α1N, of pilin subunits can abrogate and/or significantly decrease pilus assembly. I propose that electrostatic forces enable the pilin subunit to translocate from stable anchorage in the inner membrane to the growing pilus filament. To further test this hypothesis, canonical residues among Type IV pili can be changed. Glu5, located in hydrophobic N-terminal α-helix, is an invariant residue among Type IV pillins and has been shown to be essential for pilus assembly for *P. aeruginosa* and *Myxococcus xanthus*. The TCP filament model indicates that the staggered arrangement of the TcpA subunits in the helical

filaments brings each negatively charged Glu5 side chain within salt-bonding distance of the positively charged N-terminal residue, Methionine 1. These interactions may neutralize the unfavourable charges in the otherwise hydrophobic core of the filament and perhaps is pivotal in translocating pilin subunits from their membrane reservoirs into the growing filament. This study would further validate that electrostatic interactions between pilin subunits are the driving force for pilus assembly. Once assembled, it appears that the pilus stability is acquired by extensive hydrophobic interactions between hydrophobic N-terminal α-helices as indicated by TCP models. Furthermore, characterization of the integral inner membrane proteins involved in pilus assembly will provide better understanding of pilus assembly mechanisms.

By exploring the differences between the TCP from classical and El Tor biotypes, I show that key amino acid differences result in dramatically different interactions between the pili. The key determinant in pilus:pilus interaction seems to lie on the bulge (residue 156) and in the cavity (residue 113) of the TCP filament. From this result, we propose a model for pilus:pilus interactions whereby protruding regions of the filament intercalate into depressions in adjacent filaments to form tight and highly specific interactions that hold cells together in microcolonies. This pilus interaction model may also explain pilus-mediated aggregation for other bacteria. *N. gonorrhoeae* GC Type IV pili are involved in microcolony formation and GC pili also possess undulating surfaces, with protruding D-region hyper variable loops and grooves running between the globular domains (Craig *et al*., 2006). This type of pilus:pilus interaction may be

universal among Type IV pili. Complementarity between the bulge and the cavity of the filament must be explored further.

CTXϕ infection of various TcpA mutants indicates that CTXϕ attachment occurs over a large surface of the pilus. Consistent with this result, immuno-gold labelling indicates CTXϕ interact with TCP all along its surface. TEM analyses indicate the possibility of the major coat protein, Cep, as an initial binding module in TCP:CTXϕ interactions. Systematic mutations on Cep and examining the effects of such mutations on Cep in *V. cholerae* infection will test the hypothesis of Cep as an initial binding protein to TCP.

Knowing how TCP works and functions is of immense scientific interest as it will enable the design of peptide antigens that are likely to induce a protective immune response against *V. cholerae*. In the present study, owing to the availability of crystal structures of TcpA and computational filament models, a rationale mutagenesis approach was possible. This work contributes to an atomic level understanding of pilus assembly, pilus:pilus interaction and pilus:CTXϕ interaction.

APPENDICES

Appendix A: PCR primers and plasmids

Table A1 Primers used in the site directed mutagenesis

Primer	Sequence
D113A	F) 5' GCATTTGCAATTTCAGTGGCTGGTCTGACACAGGC R) 5' GCCTGTGTCAGACCAGCCACTGAAATTGCAAATGC
C120A	F) 5' GGTCTGACACAGGCTCAAGCCAAGACACTTATTACCAG R) 5' CTGGTAATAAGTGTCTTGGCTTGAGCCTGTGTCAGACC
D175N	F) 5' TCGCTCCCGCTAGTAAGAATTTAAATCTAACGAACATCACTCACG R) 5' CGTGAGTGATGTTCGTTAGATTTAAATTCTTACTAGCGGGAGCGA
K172A/D175N	F) 5' TCGCTCCCGCTAGTGCGAATTTAAATCTAACGAACATCAC R) 5' GTGATGTTCGTTAGATTTAAATTCGCACTAGCGGGAGCGA
A156D	F) 5' GAGAATTCTGCAGCAGACGCTGAGACAGGCGT R) 5' ACGCCTGTCTCAGCGTCTGCTGCAGAATTCTC
E158A	F) 5' CTGCAGCAGCGGCTGCGACAGGCGTTGGTGT R) 5' ACACCAACGCCTGTCGCAGC CGCTGCTGCAG
K172A	F) 5' TCGCTCCCGCTAGTGCGAATTTAGATCTAACG R) 5' CGTTAGATCTAAATTCGCACTAGCGGGAGCGA
D156A/E158A	F) 5' TTGAGAATTCTGCAGCAGCGGCTGCGACAGGCGTTGG R) 5' CCAACGCCTGTCGCAGCCGCTGCTGCAGAATTCTCAA
D113G	F) 5' GCATTTGCAATTTCAGTGGGTGGTCTGACACAGGC R) 5' GCCTGTGTCAGACCACCCACTGAAATTGCAAATGC
K85A	F) 5' TCATCCGATGAGGCAGCAAACCCATTCATTGGTAC R) 5' GTACCAATGAATGGGTTTGCTGCCTCATCGGATGA
A170G	F) 5' AAATCTATCGCTCCCGGTAGTAAGAATTTAGATC R) 5' GATCTAAATTCTTACTACCGGGAGCGATAGATTT
A138E	F) 5' ATATTGCAATCAAAGAAGGTGGCGCAGTAGC R) 5' GCTACTGCGCCACCTTCTTTGATTGCAATAT
K187T	F) 5' GTTGAGAAATTATGTACAGGTACTGCTCCATTC R) 5' GAATGGAGCAGTACCTGTACATAATTTCTCAAC
A156D/E158A	F) 5' GAGAATTCTGCAGCAGACGCTGCGACAGGCGTTGGTGTG R) 5' CACACCAACG CCTGTCGCAG CGTCTGCTGC AGAATTCTC
V161A	F) 5' GCGGCTGAGACAGGCGCTGGTGTGATCAAATC R) 5' GATTTGATCACACCAGCGCCTGTCTCAGCCGC
T159A	F) 5' AGCGGCTGAGGCAGGCGTTGGTGTG R) 5' CACACCAACGCCTGCCTCAGCCGCT
A102D	F) 5' TTTTTTCATTTCCGCGTAATGACGCAGCTAATAAAGCATTTGC R) 5' GCAAATGCTTTATTAGCTGCGTCATTACGCGGAAATGAAAAAA
K85E	F) 5' TCATCCGATGAGGCAGAAAACCCATTCATTGGTAC R) 5' GTACCAATGAATGGGTTTTCTGCCTCATCGGATGA
Sequencing primer	Vc-tcpa-flank-f) 5' CGCATTTCCTTTAAACACGAGTAAAATG Vc-tcpa-flank-r) 5' GCCCATTATTTAATGGGCAACGTT

Table A2 Plasmids with *tcpA* mutations

Plasmid	Mutation
pML9	D113A
pML10	C120A
pML12	D175N
pML14	K172A/D175N
pML15	A156D
pML16	A138E/A156D/E158A/k172A/K187T
pML17	E158A
pML18	K172A
pML25	pLC016 changed to D156A
pML28	D113G
pML29	K85E
pML30	K85A
pLC1	A138E
pLC6	K187T
pLC7	A156D/E158A
pLC9	A138E/A156D/E158A
pLC10	A138E/A156D/E158A/K172A
pLC11	A138E/A156D/E158A/K187T
pLC12	A156D/E158A/K172A/D175N
pLC13	A138E/A156D/E158A/K172A/D175N
pLC15	A156D/E158A/K172A/D175N/K187T
pLC16	A138E/A156D/E158A/K172A/D175N/K187T
pML21	R26E
pML22	E83R
pML23	L76K
pML24	R26E/E83R
pML2	V161A
pML8	T159A
pML11	A102D

Appendix B: PCR conditions

Table B1 QuickChange site-directed mutagenesis

1.	95°C for 5 min
2.	Add pfu polymerase
3.	95°C for 30 sec
4.	55°C for 1 min (temperature varies depending on the primer's melting temperature)
5.	68°C for 10 min (time varies depending on the size of the product: 1 min per kb)
6.	Repeat steps 3 to 5 for 19 times
7.	72°C for 5 min

Table B2 PCR reaction components for Table B1

	Final concentration
Template DNA (pTK1)	60 ng
10x pfu buffer	1x
DMSO	2%
dNTP	0.2 mM each
$MgSO_4$	2 mM
Forward primer	0.14 μM
Reverse primer	0.14 μM
pfu polymerase	1.25 unit

Table B3 PCR conditions for amplifying *tcpA* gene from *V. cholerae* chromosome

1.	95°C for 3 min
2.	Add pfu polymerase
3.	94°C for 1 min
4.	45°C for 1 min
5.	72°C for 50 sec
6.	Repeat steps 3 to 5 for 10 times
7.	94°C for 1 min
8	50°C for 1 min
9	72°C for 50 sec
10	Repeat steps 7 to 9 for 30 times

Table B4 PCR reaction components for Table B3

	Final concentration
Genomic DNA	100 ng
10x pfu Buffer	1x
DMSO	1%
dNTP	0.25 mM of each
Forward primer	0.5 μM
Reverse primer	0.5 μM
pfu polymerase	2.5 unit

Appendix C: TEM analyses of classical-to-El Tor mutants.

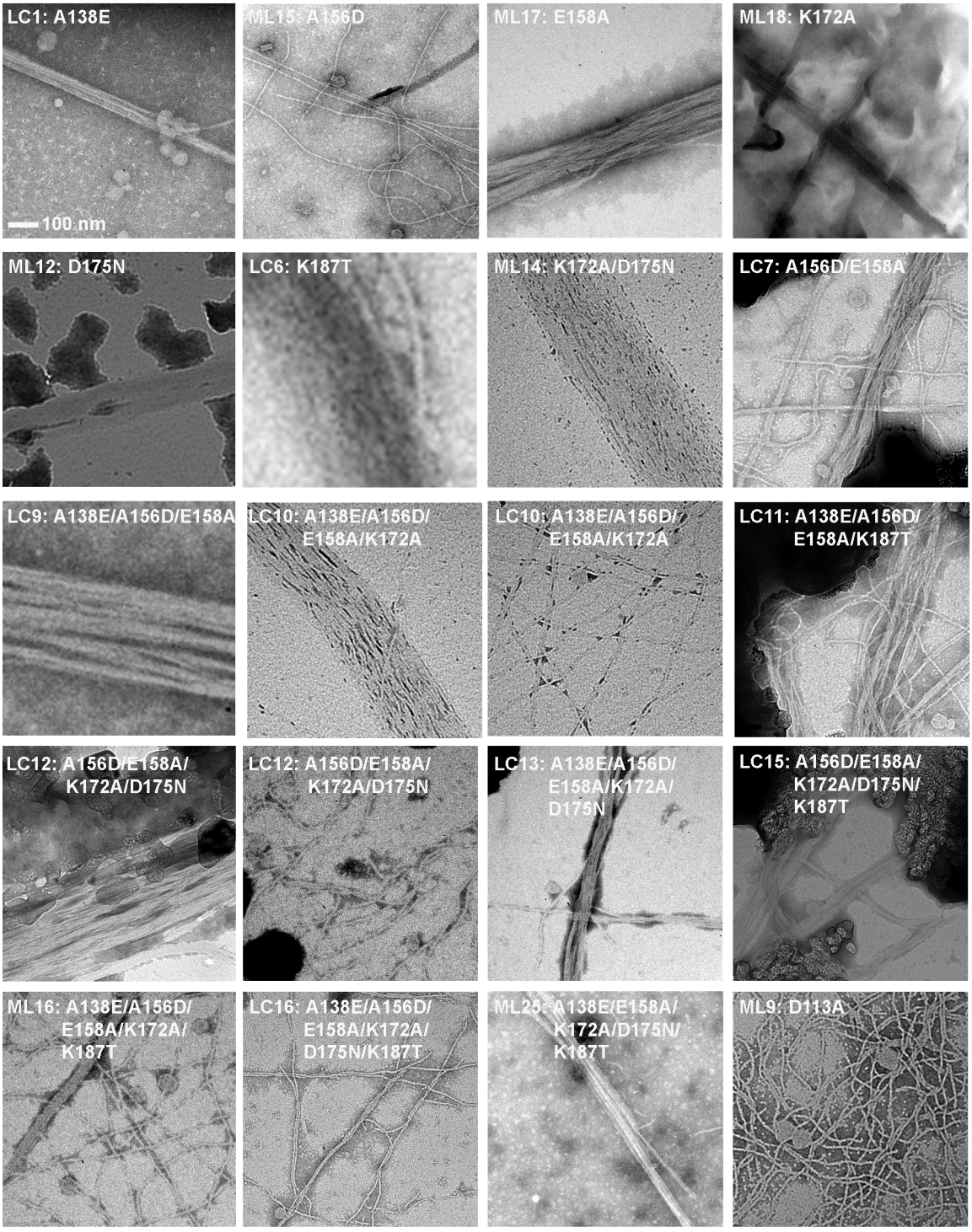

Figure C1 TEM images of classical-to El Tor mutations. Scale bar for all panels, 100 nm.

REFERENCE LIST

Barua, D., Greenough, B., History of cholera. Plenum Medical Book. New York, N.Y. 1-36 (1992).

Bieber, D., Ramer, S.W., Wu, C.Y., Murray, W.J., Tobe, T., Fernandez. R., Schoolnik, G.K. Type IV pili, transient bacterial aggregates and virulence of enteropathogenic *Escherichia coli*. *Science* **280**: 2114-2118 (1998).

Chatterjee, S. N. Chaundhuri, K. Lipopolysaccharides of *Vibrio cholerae*, physical and chemical characterization. *Biochem Biophs. Acta*. **1639**: 65-79 (2003).

Clackson,T., Lowman, H. Phage Display: A Practical approach. Oxford University Press. Oxford New York, N.Y. 2-3 (2004).

Collins, R.F., Saleem, M., Derrick, J.P. Purification and three-dimensional electron microscopy structure of the *Neisseria meningitidis* Type IV pilus biogenesis protein PilG. *J. Bacteriol.* **189**: 6389-6396 (2007).

Colwell, R., Kaper, J., Joseph. S. W. *Vibrio cholerae*, *Vibrio parahaemolyticus*, and other *Vibrios*: occurrence and distribution in Chesapeake Bay. *Science* **198**: 394-396 (1977).

Colwell, R., Huq, A. Environmental reservoir of *Vibrio cholerae*: the causative agent of cholera. *Ann. N.Y. Acad. Sci*. **740**: 44-54 (1994).

Craig, L., Taylor, R.K., Pique, M.E., Adair, B.D., Arvai, A.S., Singh, M., Lloyd, S.J., Shin, D.S., Getzoff, E.D., Yeager, M., Forest, K.T., Tainer, J.A. Type IV pilin structure and assembly: X-ray and EM analyses of *Vibrio cholerae* toxin-coregulated pilus and *Pseudomonas aeruginosa* PAK pilin. *Mol. Cell*. **11**: 1139-1150 (2003).

Craig, L., Pique, M.E., Tainer, J.A. Type IV pilus structure and bacterial pathogenicity. *Nat. Rev. Microbiol.* **2**: 363-78 (2004).

Craig, L., Volkmann, N., Arvai, A.S., Pique, M.E., Yeager, M., Egelman, E.H., Tainer J.A. Type IV pilus structure by cryo-electron microscopy and crystallography: implications for pilus assembly and function *Mol. Cell* **23**: 651-62 (2006).

Crowther, L.J., Anantha, R.P., Donnenberg, M.S. The inner membrane subassembly of the enteropathogenic *Escherichia coli* bundle forming pilus. *Mol. Microbiol.* **52**: 67-79 (2004).

Davis, B.M., Waldor M.K., CTXϕ contains a hybrid genome derived from tandemly integrated elements. *Proc. Natl. Acad. Sci. USA* **97**: 8572-8577 (2000).

Davis, B.M., Kimsey, H.H., Kane, A.V., Waldor, M.K. A satellite phage-encoded anti-repressor induces repressor aggregation and cholera toxin gene transfer. *EMBO J*. **21**: 4240-4249 (2002).

Davis, B.M., Waldor, M.K. Filamentous phages linked to virulence of *Vibrio cholerae*. *Curr. Opin. Microbiol*. **6**: 35-42 (2003).

DiRita, V., Neely, M., Taylor, R., Bruss, P. Differential expression of the ToxR regulon in classical and El Tor biotypes of *Vibrio cholerae* is due to biotype-specific control over *toxT* expression. *Proc. Natl. Acad. Sci. USA* **93**: 7991-7995 (1996).

Faruque, S., Asadulchani, Alim, A.R.M., Albert, J., Islam, N., Mekalanos, J. Induction of the lysogenic phage encoding cholera toxin in naturally occurring strains of toxigenic *Vibrio cholerae* O1 and O139 *Infec. Immun.* **66**: 3752-3757 (1998).

Faruque, S., Asadulghani, Rahman, M., Waldor, M., Sack, D. Sunlight induced propagation of the lysogenic phage encoding cholera toxin. *Infec. Immun*. **68**: 4795-4801 (2000).

Figurski, D.H., Helinski, D.R. Replication of an origin-containing derivative of plasmid RK2 dependent on a plasmid function provided in trans. *Proc. Natl. Acad. Sci. USA* **76**:1648-1652 (1979).

Freitag, N.E., Seifert H.S., Koomey, M. Characterization of the *pilF-pilD* pilus assembly locus of *Neisseria gonorrhoeae*. *Mol. Microbiol.* **16**: 575-586 (1995).

Garay, E., Arnau, A., Amaro, C. Incidence of *Vibrio cholerae* and related *Vibrios* in a coastal lagoon and seawater influenced by lake discharges along an annual cycle. *Appl. Environ. Microbiol*. **50**: 426-430 (1985).

Herrington, D.A., Hall, R., Losonsky, G., Mekalanos, J., Taylor, R., and Levine, M. Toxin coregulated pili and *toxR* regulon are essential for *Vibrio cholerae* pathogenesis in humans. *J. Exp. Med*. **168**: 1487-1492 (1988).

Higashi, D.L., Lee, S.W., Snyder, A., Weyand, N.J., Bake, A., So, M. Dynamics of *Neisseria gonorrhoeae* attachment: microcolony development, cortical plaque formation, and cytoprotection. *Infect. Immun*. **75**: 4743-4753 (2007).

Huq, A., Colwell, R., Rahman, R., Ali, A., Chowdhury, M. AA.R., Parveen, S., Sack, D. A., Russek-Cohen., E. Detection of *Vibrio cholerae* in the aquatic environment measured by fluorescent antibody and culture method. *Appl. Environ. Microbiol*. **56**: 2370-2373 (1990).

Islam, M. S., Drasar, B. S., Sack, R.B. The aquatic flora and fauna as reservoir of *Vibrio cholerae*: a review. *J. Diarrh. Dis. Res*. **12**: 87-96 (1994).

Iwanaga, M., Kuyyakanond, T. Large production of cholera toxin by *Vibrio cholerae. J. Clin. Micrbiol*. **25**: 2314-2316 (1987).

Kaper, J.B., Morris, J.G., Levine, M.M., Cholera. *Clin. Microbiol. Rev.* **8**: 48-86 (1995).

Kaufman, M.R., Jerome, M.S., Taylor, R. K. Processing of TCP pilin by TcpJ typifies a common step intrinsic to a newly recognized pathway of extracellular protein secretion by gram-negative bacteria. *Genes Dev*. **5**: 1834-1846 (1991).

Kaufman, M.R., Shaw, C.E., Jones, I.D., Taylor, R. K. Biogenesis and regulation of the *Vibrio cholerae* toxin-coregulated pilus: analogies to other virulence factor secretory systems. *Gene* **126**: 43-49 (1993).

Kimsey, H.H., Waldor, M.K. CTXϕ immunity: application in the development of cholera vaccines. *Proc. Natl. Acad. Sci. USA* **95**: 7035-7039 (1998).

Kirn, T.J., Lafferty, M.J., Sandoe, C.M., Taylor, R.K. Delineation of pilin domains required for bacterial association into microcolonies and intestinal colonization by *Vibrio cholerae*. *Mol. Microbiol.* **35**: 896-910 (2000).

Kirn, T.J., Bose, N., Taylor, R. Secretion of a soluble colonization factor by the TCP type 4 pilus biogenesis pathway in *Vibrio cholerae*. *Mol. Microbiol*. **49**: 81-92 (2003).

Li, J., Lim, M., Brock, M., Pique, M.E., Woods, V.L., Craig, L. *Vibrio cholerae* toxin-coregulated pilus structure analyzed by hydrogen/deuterium exchange mass spectrometry. *Structure* **16**: 137-148 (2008).

Maloy S.R., Stewart, V., Taylor, R. Genetic analysis of pathogenic bacteria laboratory manual. Cold Spring Harbor Laboratory Pr. 399-401 (1996).

Marceau, M., Beretti, J.L., Nassif, X. High adhesiveness of encapsulated *Neisseria meningitidis* to epithelial cells is associated with the formation of bundles of pili. *Mol. Microbiol*. **17**: 855-63 (1995).

Medrano, A.I., DiRitta, V.J., Castillo, G., Sanchez, J. Transient transcriptional activation of the *Vibrio cholerae* El Tor virulence regulator toxT in response to culture conditions. *Infect Immun*. **67**: 2178-2183 (1999).

Mekalanos, J.J. Duplication and amplification of toxin genes in *Vibrio cholerae*. *Cell* **35**:253-263 (1983).

Pearson, G.D., Woods, A., Chiang, S., Mekalanos, J.J., CTX genetic element encodes a site specific recombination system and an intestinal colonization factor. *Proc. Natl. Acad. Sci. USA.* **90**: 3750-3754 (1993).

Peek, J.A., Taylor, R.K. Characterization of a periplasmic thiol:disulfide interchange protein required for the functional maturation of secreted virulence factors of *Vibrio cholerae*. *Proc. Natl. Acad. Sci. USA.* **89**: 6210-6214 (1992).

RDI. How to choose a Gold Conjugate by BBI international. RDI division of Fitzgerald Industries Intl. USA. http://www.researchd.com/gold/pickgold.htm (1997).

Skorupski, K., Taylor, R.K. Positive selection vectors for allelic exchange. *Gene* **169**: 47-52 (1996).

Strom, M.S., Nunn, D.N., Lory, S. A single bifunctional enzyme, PilD, catalyzes cleavage and N-methylation of proteins belonging to the Type IV pilin family. *Proc. Natl. Acad. Sci. USA.* **90**: 2404-2408 (1993).

Tacket, C. O., Taylor, R.K., Losonsky, G., Lim, Y., Nataro, J.P. Kaper, J. B., Levine, M. M. Investigation of the roles of toxin coregulated pili and mannose-sensitive hemagglutinin pili in the pathogenesis of *Vibrio cholerae* O139 infection. *Infect. Immune*. **66**: 692-695 (1998).

Taylor, R., Miller, V., Furlong, D., Mekalanos, J. Use of *phoA* gene fusion to identify a pilus colonization factor co-ordinately regulated with cholera toxin. *Proc. Natl. Acad. Sci*. USA. **84**: 2833-2837 (1987).

Taylor, R.K., Kirn, T.J., Meeks, M.D., Wade, T.K., Wade, W.F. A *Vibrio cholerae* classical TcpA amino acid sequence induces protective antibody that binds an area hypothesized to be important for toxin-coregulated pilus structure. *Infect. Immun*. **72**: 6050-6060 (2004).

Tripathi, S.A., Taylor, R.K: Membrane association and multimerization of TcpT, the cognate ATPase ortholog of the *Vibrio cholerae* toxin-coregulated pilus biogenesis apparatus. *J. Bacteriol*. **189**: 4401-4409 (2007).

Wachsmuth, I. K., Olsvik, O., Evins, G. M., Popovic, T. Molecular epidemiology of cholera. *Vibrio cholerae* and cholera: molecular to global perspectives. American society for microbiology. 375-380 (1994).

Waldor, M.K., Mekalanos, J.J. Lysogenic conversion by a filamentous phage encoding cholera toxin. *Science* **272**: 1819-1914 (1996).

Waldor, M.K., Rubin, E.J., Pearson, G.D., Kimsey, H., Mekalanos, J.J. Regulation, replication and integration function of the *Vibrio cholerae* CTXϕ are encoded by region RS2. *Mol. Microbio*. **24**: 917-926 (1997).

Waldor, M.K., Heilpern, A.J. $pIII^{CTX}$, a predicted CTXphi minor coat protein, can expand the host range of coliphage fd to include *Vibrio cholerae. J. Bacteriol.* **185**: 1037-1044 (2003).

WHO. Cholera vaccines. Wkly Epidemiol. *Record* **76**: 117-124 (2001).

WHO. Cholera 2006. *Wkly Epidemiol. Record* **82**: 273-284 (2007).

WHO. Cholera, Zimbabwe. *Wkly Epidemiol. Record* **83**: 449-460 (2008).

WHO. Global, national efforts must be urgently intensified to control Zimbabwe cholera outbreak. http://www.who.int/mediacentre/news/releases/2009/cholera_zim_20090130/en/index.html (2009).

Zhang, H.A., Donnenberg, M.S. DsbA is required for stability of the Type IV pilin of enteropathogenic *Escherichia coli. Mol. Microbiol.* **21**: 787-797 (1996).